Scientific Reports

https://doi.org/10.1038/s41598-026-48936-y

Article in Press

Evaluating the binder performance and biocomposite applications of thermally reactivated wood-wool cement panel waste

Received: 28 January 2026

Accepted: 10 April 2026

Published online: 21 April 2026

Cite this article as: Argalis P.P., Vitola L., Puzule L. *et al.* Evaluating the binder performance and biocomposite applications of thermally reactivated wood-wool cement panel waste. *Sci Rep* (2026). https://doi.org/10.1038/s41598-026-48936-y

Pauls P. Argalis, Laura Vitola, Liga Puzule, Xiangming Zhou, Maris Sinka & Diana Bajare

Evaluating the binder performance and biocomposite applications of thermally reactivated wood-wool cement panel waste

Pauls P. Argalis[1, *][0000-0002-1840-8202], Laura Vitola[1][0000-0002-8169-3878], Liga Puzule[1][0009-0009-6333-9259], Xiangming Zhou[2][0000-0001-7977-0718], Maris Sinka[1][0000-0002-2332-1347], Diana Bajare[1]

[1]Institute of Sustainable Building Materials and Engineering Systems, Faculty of Civil and Mechanical Engineering, Riga Technical University, Kipsalas Street 6A, LV-1048, Riga, Latvia

[2]Department of Civil & Environmental Engineering, Brunel University London, Uxbridge UB8 3PH, UK

Corresponding author: Pauls-Pavils.Argalis@rtu.lv, Kipsalas 6A, LV-1048, Riga, Latvia

Abstract: This study addresses a research gap in upcycling complex organic-mineral residues by investigating the thermal reactivation of sanding dust (SD) generated during the production of wood-wool cement panels. Its novelty lies in establishing a low-temperature pathway that recovers hydraulic capacity without triggering CO_2 release from carbonated phases. The research design involved heating raw SD at 450 ℃ for five hours - a temperature selected to maximize portlandite dehydration while remaining below the 600 ℃ decarbonation threshold - followed by comprehensive chemical, mineralogical, and physical characterization (XRD, TGA, SEM). This reactivated binder was then utilized to produce novel, low-density biocomposites using manufacturing-line waste as filler. Major findings confirmed that heat treatment reduced average particle size from 29.21 µm to 19.11 µm and successfully restored hydraulic activity, increasing binder compressive strength from 1.59 to 13.05 MPa. The resulting biocomposites achieved compressive strengths up to 185 kPa and a low thermal conductivity of 0.068 W/(m·K) with a density of 369–415 kg/m^3. These results indicate that 450 ℃ serves as an optimal "thermal window" for this waste, effectively transforming industrial residues into functional secondary raw materials for sustainable building insulation.

Keywords: Wood-wool cement panel; cement reactivation; thermal treatment; sustainable building materials; circular manufacturing; life cycle assessment.

1. INTRODUCTION

Researchers focus more on the reactivation and recycling of Portland cement-based binders, especially from cement-based production waste, as the need for sustainable materials increases [1,2]. By reactivating the binding properties of partially hydrated cementitious materials, this technical strategy aims to convert waste into useful building material resources [3,4]. The industry could tackle major environmental issues, such as waste generation, resource depletion, and carbon emissions, by putting reactivation technology into practice [5]. This approach represents a promising pathway to mitigate the environmental

degradation associated with traditional cement production, offering a more sustainable alternative to conventional material extraction and manufacturing processes [6].

1.1. Environmental Impact of the Construction Materials Sector

The construction industry has a significant impact on the environment and global resource consumption, with substantial implications for sustainability. The building and construction industry is accountable for 33 % of energy-related CO_2 emissions, according to the International Energy Agency's global status report [7]. This number highlights the crucial role in mitigating climate change, including operating emissions (26%) and embodied carbon emissions from materials and construction processes (7%) [8].

When it comes to sustainability, trends in construction materials are especially troubling. Construction materials account for approximately half of all raw materials extracted worldwide, according to the United Nations Environment Programme’s report on resource efficiency and climate change [9]. In this context, the production of concrete is a major environmental concern, accounting for approximately 8 % of global CO_2 emissions (Fig. 1) and producing more than 4 billion tons of cement annually [1,10].

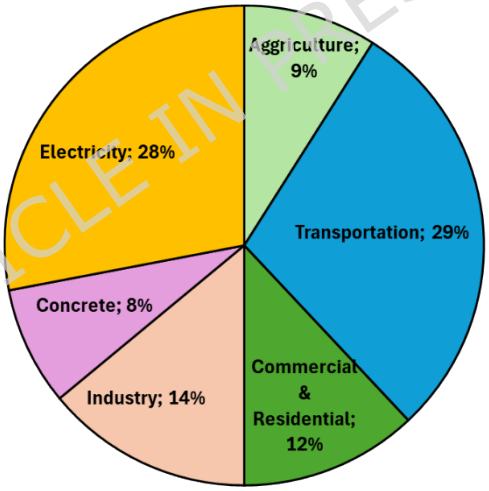

Figure 1. Concrete production global CO_2 emissions [10].

1.2. Reactivation by Heat Treatment

Cement recycling has also focused on reactivating the binder through heat treatment. Heat treatment techniques aim to change the cement's physical and chemical properties and restore the cement's activity, thereby reducing the need to use newly manufactured cement [11].

The opportunities offered by heat treatment are significant in terms of sustainability and resource-saving. The recovery and reuse of cement can reduce the demand for raw materials, thereby reducing energy consumption, greenhouse gas emissions, and the overall environmental impact of cement production [12]. In addition, it can potentially reduce construction and

demolition waste by diverting it from landfills and using a circular economy approach [13].

Various heat-treatment methods are being explored in cement recycling to reactivate the binder. Pyrolysis, a process involving applying high temperatures without oxygen, can break down organic matter and remove contaminants, thus recovering a clean cement paste [14]. Calcination, conversely, involves heating cementitious materials at high temperatures to induce chemical changes that release carbon dioxide and recover reactive calcium compounds [15]. Incineration, a more extreme heat treatment, removes organic matter and impurities and uses the energy released during combustion [16].

The reactivation of cement binders has gained significant attention in recent years as a promising approach to reducing environmental impact and resource consumption in the construction industry [17,18]. Among various thermal treatment technologies, muffle furnaces and rotary kilns have emerged as promising options due to their versatility, precise temperature control, and scalability [19]. While muffle furnaces are widely used in laboratory-scale investigations due to their excellent temperature uniformity and controlled atmosphere, rotary kilns offer advantages in continuous operation and industrial-scale processing, making them suitable for large-scale cement reactivation applications [20]. Microwave heating has attracted significant attention due to its unique ability to selectively heat material components. Choi et al. [21] demonstrated that microwave treatment can effectively reactivate hydrated cement paste, increasing its compressive strength by up to 30% compared to untreated samples. The mechanism involves selective molecular vibration and dielectric heating, which can more efficiently redistribute moisture and activate chemical bonds than traditional heating methods.

In cement reactivation applications, muffle furnaces play a vital role in studying various cement types' thermal behaviour and reactivation potential, where controlled heating environments are essential for investigating phase transformations and chemical reactions [22]. Research has shown that cement materials subjected to thermal treatment in muffle furnaces at temperatures ranging from 400 °C to 900 °C exhibit significant changes in their mineralogical composition and reactivity, with optimal reactivation temperatures varying depending on the cement composition and initial conditions [22,23]. The precise temperature control and uniform heat distribution characteristics of muffle furnaces make them particularly suitable for studying the dehydration and rehydration processes in cement materials and investigating the formation of new phases during thermal treatment [24]. Using lower temperatures (< 600 °C) in that range dehydrates the cementitious phases but doesn’t reach the calcium carbonate decomposition temperature, which would produce emissions. By encapsulating calcium carbonate and focusing only on cementitious phases, a reactivated cementitious binder can be developed.

Despite the progress in circular construction, a significant scientific gap persists regarding the selective reactivation of industrial cementitious byproducts compared to conventional construction and demolition waste (CDW). Current literature predominantly focuses on the mechanical and thermal processing of recycled concrete aggregates (RCA), where the primary objective is the removal of adhered mortar or the enhancement of aggregate properties

rather than the reactivation of the cement paste fraction itself [25,26]. While recent studies have extensively explored geopolymerization as a dominant pathway for upcycling construction debris, sand-washing waste, and autoclaved aerated concrete into sustainable binders [27–32], these systems often rely on external chemical alkaline activators or alumina-silicate bases to achieve structural integrity. This leaves a gap in the research regarding how thermal reactivation can selectively recover the inherent hydraulic capacity of complex, organic-mineral residues - such as wood-wool cement panel sanding dust - without inducing fiber degradation or the release of CO_2 from carbonated phases. Unlike the inert mineral matrices found in RCA, industrial residues from wood-wool cement panel production contain significant organic fibers that alter thermal kinetics and mineralogical transformations during heating. Furthermore, while low-carbon ternary binders and accelerated carbonation have shown promise in biocomposite development [33], the direct transformation of manufacturing-line waste into a self-binding secondary raw material via low-temperature (450 ℃) treatment remains under-researched. This study, therefore, shifts the scientific narrative from aggregate-centric recycling to the precise mineralogical restoration of industrial paste-rich waste, establishing a circular pathway that avoids the chemical intensity of geopolymerization while maintaining the carbon-sequestering benefits of the stable calcite structure.

1.3. Environmental and Economic Considerations

Transitioning to a circular economy within the construction sector necessitates innovative binder reactivation strategies. While cement recycling through thermal treatment is promising, its industrial integration depends on overcoming challenges related to scalability and economic viability [15,34]. Although advanced heating technologies require significant initial investments - ranging from 0.25 to 1.5 million € - optimized reactivation processes can yield 20–40 % savings in material procurement costs compared to traditional manufacturing [34,35].

The scientific mechanism of reactivation involves the thermal dehydration of hydrated compounds, which restores binding capacity upon subsequent rehydration [13]. However, the intensity of this treatment dictates a critical trade-off between binder quality and environmental impact. For instance, "re-clinkering" end-of-life cement at approximately 1450 ℃ restores complete hydraulic capacity but exceeds the decarbonation threshold (600–750 ℃), releasing stored CO_2 unless expensive capture technologies are employed [34].

Conversely, low-temperature reactivation at 450 ℃ offers a sustainable alternative for carbon-sensitive waste streams [36]. By remaining below the decarbonation limit, this method selectively converts portlandite into reactive precursors while maintaining calcite stability, thereby sequestering carbon within the material structure [37]. This approach minimizes process emissions while providing sufficient binding properties for specialized applications such as low-density biocomposites.

Despite this potential, significant knowledge gaps persist regarding energy-efficient scaling, long-term material performance, and the development of hybrid activation methods [38–40]. These gaps are particularly evident in the wood-wool cement panel (WWCP) industry. With an annual global production of 174 million m^2, the industry generates over 450,000 m^3 of waste, much of which consists of sanding dust (SD)—a composite residue of wood fibers and partially hydrated cement currently destined for landfills [41,42].

This research addresses this industrial waste management challenge by investigating the upcycling of sanding dust from a Latvian WWCP plant. By employing a 450 °C thermal treatment, this case study characterizes the resulting binder's properties and evaluates its performance in novel, low-density biocomposites. This approach demonstrates how manufacturing residues can be transformed into more environmentally friendly secondary raw materials, contributing to resource conservation and a reduced ecological footprint for the construction industry.

2. MATERIALS AND METHODS

2.1. Raw Materials

This study's raw materials are generated in a Latvian wood-wool cement panel manufacturing plant. Sanding dust (SD) is generated in the sanding phase of WWCP and will be used to develop the binder. The filler material is generated at the starting processes of WWCP manufacturing.

2.1.1. Binder Precursor - Sanding Dust

Cured and dried wood-wool cement panels undergo cutting, edge treatment, and size calibration by sanding in the final stage of production. To reduce potential health risks from airborne dust during sanding, a dust extraction system (Fig. 2) minimizes dust and keeps the workspace clean.

Figure 2. Sanding dust extraction system; 1) panel treatment facility with cutting and sanding equipment; 2) Dust filters and separators; 3) sanding dust storage room [43,44].

Figure 3 illustrates the interior of the sanding dust (SD) storage room. The continuous grinding and filter-cleaning processes produce about 4-5 m^3 of SD daily.

Figure 3. SD was generated during the manufacturing of the wood-wool cement panels.

The final sanding step is critical for achieving the desired surface finish during wood-wool cement panel manufacturing. This sanding process generates dust particles, and understanding their morphology is essential for occupational health and safety and process optimisation. The SD primarily consists of two key components: wood fibre and partially hydrated cement particles. Wood fibre particles are typically elongated and fibrous, resembling strands or flakes. Their morphology can vary based on wood species, fibre processing, and board manufacturing methods [44].

Cement particles, on the other hand, are typically much finer and appear as tiny, asymmetrical grains or pieces. The type, fineness, and hydration state of cement all affect the shape of cement particles.

From larger, more visible coarse particles to tiny particulates that could become airborne, the size distribution of SD particles can vary widely. Because of their size and weight, coarse particles tend to settle quickly. Fine particles, on the other hand, may linger in the air for prolonged periods, posing breathing risks that call for countermeasures such as dust extraction devices.

Additionally, because of electrostatic forces or moisture absorption, SD particles - especially finer particles - may cluster or agglomerate.

The granulometric composition of the SD was determined by sieving according to ASTM C136 [45] before the processing. The sizes range from 0.125 mm to 8 mm. Figure 4 summarises the average granulometric composition of the SD as a green-shaded area, with the average distribution indicated by a

dashed line. The analysis shows that approximately 31 % (± 8.5 %) of the material consists of the finest fraction (0-0.125 mm). The fraction 0.125-0.25 mm comprises about 26 % of the material, bringing the cumulative passing percentage to 57 % (± 9.2 %) for particles under 0.25 mm. Moving up in size, the 0.25-0.5 mm fraction contains roughly 18 % of the material, and the 0.5-1 mm fraction adds another 15 %, bringing the total passing to approximately 90 % (± 5.9 %) for particles under 1 mm. The remaining fractions contribute minimally to the overall distribution, with particles between 1-8 mm making up about 10 % of the total material. The shaded area in the graph represents the variation in particle size distribution, with the greatest spread observed in the middle range (0.125-0.5 mm). This analysis indicates that the sanding dust predominantly comprises particles smaller than 1 mm, with the majority falling below 0.5 mm.

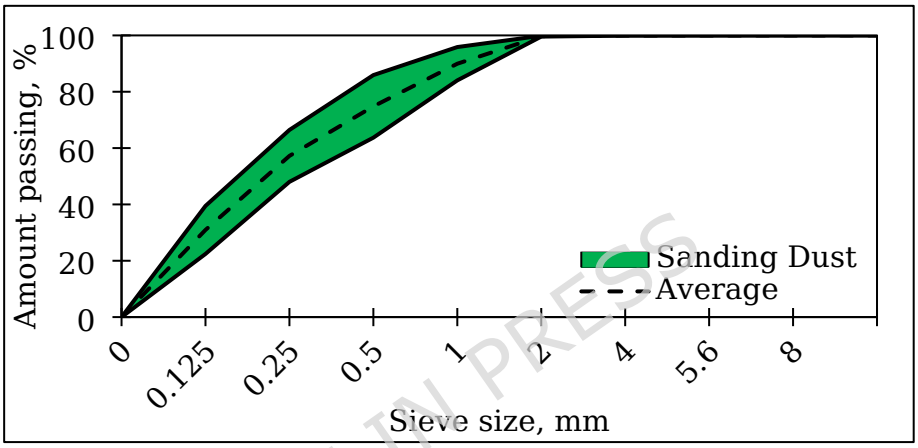

Figure 4. Granulometric composition of the sanding dust.

Figure 5. shows the visual appearance of each fraction of SD. In figures 5a, b, and c, large wood particles with cement conglomerates can be observed. In figures 5g and 5h, a distinct powdery material can be observed, a mixture of fine cement and wood particles.

Figure 5. The appearance of sand dust by a fraction (a) 5.6-8 mm; (b) 4-5.6 mm; (c) 2-4 mm; (d) 1-2 mm; (e) 0.5-1 mm; (f) 0.25-0.5 mm; (g) 0.125-0.25 mm; (h) 0-0.125 mm.

As this waste material contains both hydrated and unhydrated cement, the aim is to reactivate the hydrated cement binder through heat treatment to regain the material's cementitious properties and utilise it as a binder to produce biocomposites.

2.1.2. Filler - Production Line Waste

Production Lined Waste (PLW) is generated when the wood-wool and cement mixture goes through a conveyor system in the manufacturing plant. After each shift, these conveyors are cleaned, and the material that sticks to the belts is discarded as waste. The composition is like the primary production product – acoustic wood-wool cement panel. The difference is that one is pressed into a board form, while the other remains a loose material. This loose material can be used as a filler and offers several benefits over other natural fillers. As it consists of wood-wool coated in cement, the fibres are brittle and not prone to rot. The visual appearance of the filler material is shown in Figure 6.

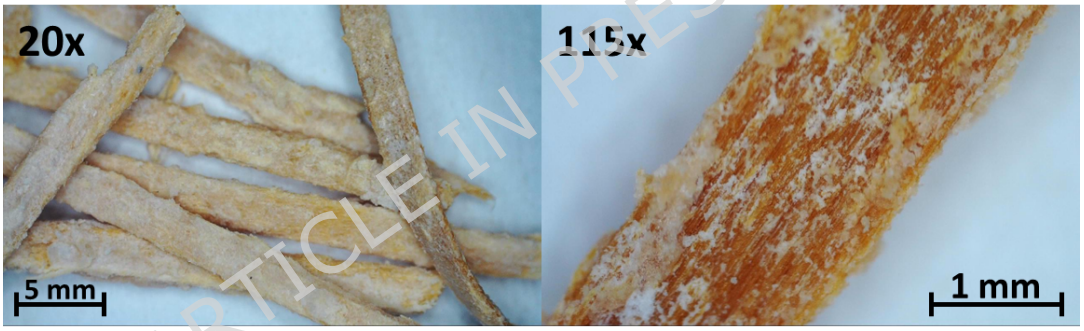

Figure 6. Visual appearance of the filler material [41].

2.2. Reactivation Method

The sanding dust fraction was reactivated in a muffle furnace by heating the material to 450 ℃ at 10 ℃/min and holding it at that temperature for 5 hours. The temperature was chosen based on previous DTA results [1], which showed that a peak in the dehydration of the portlandite phase occurred around 450 ℃. A muffle furnace was used to control the temperature, and the holding time at that temperature was selected based on prior experience to ensure that all the organic material decomposed [1,2,26,44]. The resulting material is a grey-coloured powder that contains wood coal particles and dehydrated cement phases. The main limitation of the study is the use of a muffle furnace, as in an industrial setting, reactivation would likely be performed in a rotary kiln or a fluidized bed reactor. The thermal kinetics of how fast the material heats up and

how evenly the heat is distributed would be a different large-scale system, potentially affecting the mineralogical consistency of the HTSD.

2.3. Mix Design and Sample Preparation

2.3.1. Of Binder

The reference series in this study was untreated sanding dust, used as a baseline for comparing data to understand how the heat treatment affected the waste. The sanding dust was sieved through a 250 µm sieve to obtain a more homogeneous mixture and to reduce the amount of wood particles. This sieved mixture was combined with water to make the paste samples. No additional binders were used in this study.

For both sample series, the mix design was similar. For the reference sample (SD), a W/B ratio of 0.7 was used to achieve a workable material. Similarly, for the HTSD, a W/B ratio of 0.73 was used. No plasticisers or other additives were used in this study.

The required amount of water and material was weighed and added to the mixing bowl of the Hobart N50 planetary mixer, with the water added first. The mixer was set to the lowest speed setting (~140 RPM) and mixed for 2 minutes. The mixture was stirred with a spoon to evenly distribute the material in the mixing bowl, then continued mixing until homogeneous (2-3 minutes). The mortar paste was moulded into a ring for the setting time test using the Wick apparatus and into 20 x 20 x 20 mm silicon moulds for the compressive strength tests. The moulds were covered with a plastic film.

The reference samples were cured in a climate chamber (23 ± 2 ℃ and > 90% RH) above the water line, as they would disintegrate upon contact with water and would not be suitable for the tests. The HTSD samples were cured in the same climate chamber, but submerged. Samples were taken out for the compressive strength test on the 2nd, 7th, and 28th days. For each curing time, 3 parallel samples were used for data correction.

2.3.2. Of Biocomposites

Three biocomposite compositions were created, each with a different binder content. Table 1 presents the mixture design. Based on preliminary experiments and prior experience with these materials, three biocomposite series were produced [1,2,44]. The mix design for H14 was developed to achieve the lowest density and thermal conductivity while maintaining a self-bearing biocomposite. H12 was designed to achieve low load-bearing properties.

Table 1. Mix design of heat-treated binder bio-based composites.

Binder	Filler

Sample	HTSD	Water	Dry	Water for wetting*
H12	1.00	0.60	2.00	0.60
H13	0.67	0.40		
H14	0.50	0.30		

**The filler was moistened before mixing so that the filler did not absorb the water intended for the binder*

Sample preparation for biocomposites is as follows. To facilitate easier binder mixing, the fibre surface was wetted with a water-to-fibre mass ratio of 0.6. Water and filler were hand-mixed for three minutes to ensure all the fibres were moist. To achieve a homogeneous coating of the fibres, a variable mass of binder (1.00, 0.67, or 0.50 mass parts) was added to the wet filler gradually while mixing until the mix was homogeneous. The water required for the binder was then added to the mixture and mixed thoroughly. The W/B ratio for each composition was set at 0.6. Subsequently, the mix was formed in 35 cm × 35 cm × 10 cm oiled moulds.

To ensure pressure and a smoother surface structure, a plate was placed on top of the mixture after it was produced. An initial pressure of 571 Pa was applied to the samples to strengthen the bond between the binder and the wood fibers. A weight was placed on the samples to maintain a secondary pressurization of 65 Pa during curing, after the initial 60-second pressurization. After 7 days, the samples were demoulded, wrapped in plastic film, and cured for an additional 21 days to minimise humidity loss during the curing process.

2.4. Characterisation Techniques

Granulometry of dust was performed according to ASTM C136 [45] standard with a mesh size of 0.125 mm to 8 mm.

The specific surface area of the cementitious materials was determined using the Blaine air permeability method, as specified in standard EN 196-6. This technique measures the fineness of the cement by quantifying the time required for a fixed volume of air to pass through a compacted bed of the material.

Using a Veho HDMI Dual Vision Digital Scope, the macrostructure of the samples was photographed at 20× and 115× magnifications, respectively.

The samples' morphology and microstructure were examined using a Hitachi TM3000 tabletop scanning electron microscope (SEM). It does not require a conductive coating to image non-conductive materials thanks to its low-vacuum mode. A range of imaging and analysis detectors is included in the microscope's large chamber, which can hold samples up to 70 mm in diameter and 50 mm in height. SEM examination gave important information about the samples' microstructural characteristics.

A Mettler-Toledo TGA1/SF thermogravimetric analysis device was used to evaluate the thermal properties of the raw materials. At the same time,

thermograms were produced using the Mettler STARe program, which enabled the measurement of mass changes and the emission of degradation products. The analysis was conducted in an oxygen-rich environment at temperatures ranging from 25 to 800 ℃, with a heating rate of 10 ℃/min. The mass of the sample used in the experiment was approximately 10 mg.

The chemical composition of the reference sanding dust (SD) and heat-treated sanding dust (HTSD) was determined using X-ray Fluorescence (XRF) analysis. This technique was used to quantify the main oxides in the samples and to identify changes in elemental distribution resulting from the 450 °C thermal treatment. The analysis provides the material's bulk chemical composition, reported as weight percentages of the primary oxides.

A BRUKER-AXS D8 ADVANCE X-ray diffractometer (Bruker, Billerica, MA, USA) characterised the dust using CuK1 and CuK2 radiation at a 2θ range of 5–70°. The phase composition of the materials was analysed using X-ray diffractometer software (XRD; X'Pert PRO, PANalytical, Netherlands) operating at 40 kV and 30 mA with Cu Kα1 radiation (λ = 1.5406 Å).

To avoid air entrapment, the material was mixed in a moistened cone on an ASTM C143 [46] impact table and compacted. After raising the cone, the material's viscosity was determined. Additionally, the cone's height and diameter were measured. Twenty jolts were made on the impact table, producing twenty vertical drops. The cone's response to this force is observed. Measurements of the cone's diameter were used to determine its viscosity.

In accordance with EN 12667, the coefficient of thermal conductivity was determined using the LaserComp heat flow measurement device FOX 600.

Samples measured 350 × 350 mm with a thickness of 49-54 mm. The temperature difference between the plates was maintained at 20 ℃ (0 and 20 ℃). The heat transmission coefficient was derived from a continuous heat flow across the sample's surfaces. Thermal conductivity values are provided as upper and lower limits, with the average values used for data analysis.

The Zwick Z100 universal testing equipment (ZwickRoell, Kennesaw, GA, USA) was used to assess the compressive strength of the developed binder for samples measuring 2 × 2 × 2 cm at a test speed of 0.5 mm/min. The volume and density of the material were measured before the cubic samples were crushed. The compressive strength was calculated using the force applied to the sample's specific surface area.

The evaluation was conducted perpendicular to the forming direction across three parallel samples to mitigate variability, in accordance with EN 196-1:2016, with modifications to the sample size and testing times. Testing was conducted on days 2, 7, and 28 to assess the progression of compressive strength. Due to insufficient curing, a 24-hour testing duration was unfeasible as it would risk defects during demoulding.

Three samples per direction were used to assess the biocomposites' compressive and flexural strengths in two directions: parallel to and

perpendicular to the forming direction. Prismatic samples measuring 4 × 4 × 16 cm had their flexural strength evaluated, while cubic samples measuring 5 × 5 × 5 cm had their compressive strength measured. The compressive strength was measured in the parallel direction using an ultimate load. In the perpendicular direction, loads of 10 % and 20 % of the sample's height were applied.

2.5. Life Cycle Assessment

The Life Cycle Assessment (LCA) method was used to evaluate the environmental impact of the created materials. SimaPro was used to do calculations using the Ecoinvent 3.8 database. Comparing the biocomposites' thermal insulation properties to those of currently used insulation materials was the main objective. The binder's functional unit was established at 1 m^3. Based on a U-value of 0.18 W/(m^2K) per m^2 for either wall assembly or biocomposite, a functional unit was selected for biocomposites to compare their thermal insulation efficacy.

For this study, only two manufacturing scenarios were assessed, which are described in Table 2. The first scenario involves SD heated at 450 ℃ for 5 hours (HTSD), and the second scenario involves a commercial cement (CEM II/A-LL 42.5 N, Schwenk, Latvia) for data comparison. CEM II/A-LL 42.5 N was selected as the commercially available binder for the production of biocomposites that have been characterized in articles by Bumanis and Argalis [2,26]. The CEM II data were taken from the EPD of the product [47]. In this study, the environmental impact of the WWCP waste products (PLW and SD) was assumed to be zero, meaning the impact of the developed materials stems solely from other components. The results of the climate change impact are derived from the EN 15804 + A2 Method V1.03. The system boundaries included the product stage from A1 to A3. The primary limitation of this LCA is the energy consumption associated with production processes. Currently, this biocomposite is in development and produced on a laboratory scale; however, in the best-case scenario, it would be produced on an industrial scale onsite at the Latvian wood-wool cement panel manufacturing plant. Industrial-scale energy consumption data is needed to compare developed materials with traditionally used materials and obtain comparable results.

Table 2. Scenarios for the manufacturing of materials

Binders Scenario	Description
HTSD	The SD was heated for 5 hours at 450 ℃.
CEM II/A-LL 42.5 N	CEM II cement was purchased and transported from *Brocēni*, Latvia.

For the biocomposites interpolation and extrapolation method [48–54] was used to normalize the compressive strengths to achieve 3 distinct compressive strength scenarios:

- 0.05 MPa – non-load-bearing middle-layer material of a sandwich-type panel.
- 0.15 MPa – compressive strength according to EN 996, representing other biobased building materials.
- 0.50 MPa – low-load bearing construction block.

It was assumed that all material manufacturing occurred within the manufacturing plant in Jaunlaicene, Latvia; therefore, transportation was considered only for CEM II. The input data for the environmental evaluation of the developed materials is provided in Table 3. Because the heating process hasn't been widely researched for this temperature and material, a total of 9 articles were analyzed to determine the average emissions.

Table 3. Inventory data for environmental evaluation

Inputs	Mix design					
	450 (0.05)	450 (0.15)	450 (0.50)	CEM (0.05)	CEM (0.15)	CEM (0.50)
Water, kg	48	70	148	20	31	70
PLW, kg	274	256	193	301	299	294
HTSD, kg	80	117	247	-	-	-
CEM II, kg	-	-	-	5	79	176
Transport, km	-	-	-	299	299	299
Heat, kg CO_2 eq. [55–63]	26.67	39.00	82.34	-	-	-

Input data from Ecoinvent or other sources used for calculations in SimaPro is shown in Table 4. The data from the database were selected according to the geographical principle; given that local data (specific to Latvia) were not available, European data (marked as {Europe without Switzerland} or {RER} in the database) was used.

Table 4. Input data in SimaPro for environmental evaluation

Raw material	Input data from Ecoinvent
CEM II/A-LL 42,5R	*EPD* [47]
PLW	*Considered as a waste product with zero impact*
SD	*Considered as a waste product with impact from pretreatment (heating)*
Water	Tap water {Europe without Switzerland}| market for | Cut-off, U

Transport	Transport, freight, lorry 16-32 metric ton, euro5 {RER}| market for transport, freight, lorry 16-32 metric ton, EURO5 | Cut-off, U
Heat	Emissions to air, climate change - fossil

3. RESULTS AND DISCUSSION

3.1. Properties of the Binder

3.1.1. Physical Properties

The SD (Fig. 7) sample shows larger particles across the entire distribution range. 90 % of the SD sample has an average particle size of 74.89 µm, 50 % of 16.61 µm, 10 % of 0.95 µm, and an average particle size of 29.21 µm. The size difference is due to the combined hydration products and wood particles. The difference would affect the material's reactivity and performance in cement applications, as smaller particles generally provide greater surface area for hydration reactions [64].

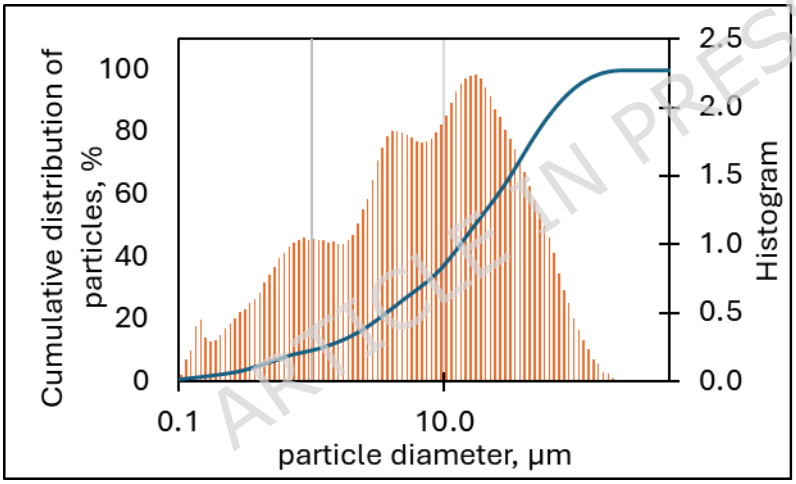

SD	
D_{10}, µm	0.95
D_{50}, µm	16.61
D_{90}, µm	74.89
Average particle size, µm	29.21

Figure 7. Cumulative particle distribution for SD.

Heat treatment at 450 ℃ (Fig. 8) reduces the overall particle size compared to SD. 90 % of the HTSD particles are up to 48.10 µm, 50 % are up to 12.46 µm, and 10 % are up to 0.47 µm. The average particle size was 19.11 µm, 35 % smaller than SD. As thermal treatment at this temperature causes partial decomposition or structural changes in the SD, particle morphology has also been affected.

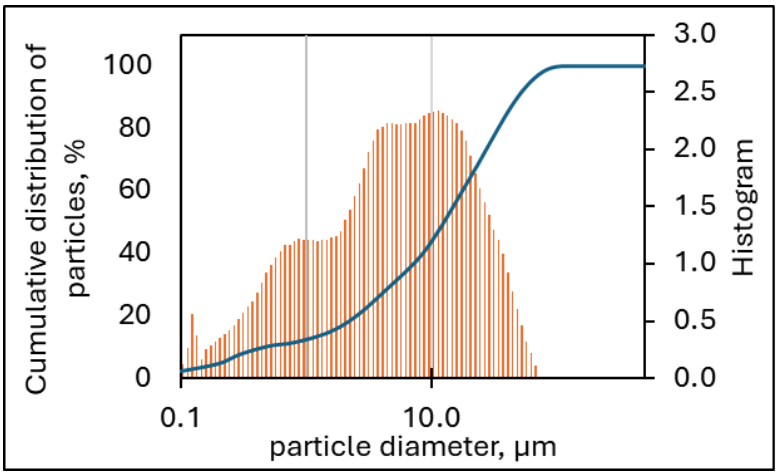

HTSD	
D_{10}, μm	0.47
D_{50}, μm	12.46
D_{90}, μm	48.10
Average particle size, μm	19.11

Figure 8. Cumulative particle distribution of HTSD.

The binder's fineness, a critical reactivity factor, was evaluated using Blaine's surface analysis. The results showed an increase in specific surface area after thermal treatment, rising from 2420 cm²/g for the reference sanding dust (SD) to 2996 cm²/g for the HTSD. This 24 % increase in surface area is a direct consequence of the physical and morphological changes induced by the heating process and is corroborated by both granulometry and microscopy findings.

The primary driver for the increased surface area is the reduction in particle size. Particle size analysis revealed that the average particle diameter decreased by 35 %, from 29.21 μm in the SD sample to 19.11 μm in the HTSD sample. This pulverisation effect, in which larger particles are broken down into smaller ones, inherently increases the powder's surface-area-to-volume ratio. Furthermore, the morphological analysis from SEM imaging provides a deeper insight. The original SD particles were described as heterogeneous conglomerates of elongated wood fibres and irregular hydrated cement particles. After heat treatment, the SEM images show that the organic wood fibres were removed, leaving an inorganic residue with a notably more porous, granular, and interconnected microstructure. This development of internal porosity and a rougher surface texture on the individual particles further contributes to the overall specific surface area measured by Blaine's method. Therefore, the combined effect of a smaller average particle size and a more porous particle morphology synergistically enhanced the fineness of the HTSD, a key factor in its improved chemical reactivity and setting performance.

3.1.2. Morphological Analysis

The macrostructural images of SD are presented in Fig. 9 at 121× magnification. In the 500-1000 μm fraction (Fig. 9a), large wood fibres dominate the composition of the SD, although some cement conglomerates can be noted, as the particle size reduces through fractions 250-500 (b) and 200-250 (c). There is more homogeneity among shorter wood fibres and white cement particles. The 125-200 μm (d) and 63-125 μm (e) fractions contain progressively finer cement

particles with wood fibre gradually more uniformly dispersed. The most minute 0-63 µm fraction of the material (f) takes on the nature of rfiner particles, shows the transformation of the waste material from bulky particles to small, homogeneous particles. This suggests that the finest fraction is likely to be the most reactive due to its structural characteristics, as it contains more cement particles and a greater surface area.

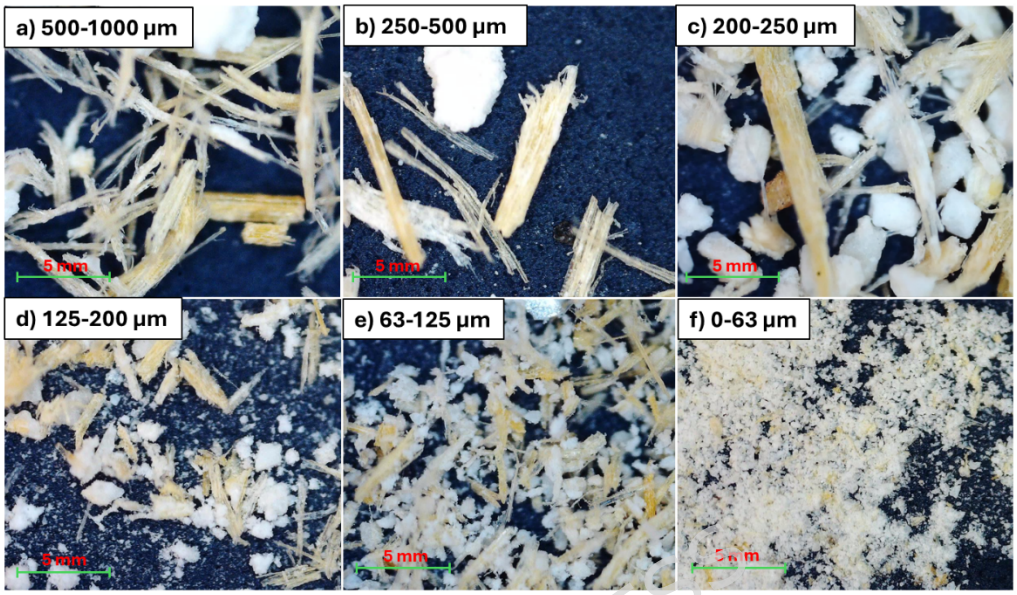

Figure 9. The visual appearance of SD at 121 times magnification.

In Figure 10, heat-treated sanding dust is shown at four different size fractions at a magnification of 121×. The 200-350 µm fraction (Fig. 10a) exhibits visible, coarse, irregularly shaped particles ranging from dark brown to light tan, indicating differences in the effects of heat treatment. In the 125-200 µm fraction (Fig. 10b), the individual particles are relatively small but still perceptible. The colour range of such particles is about the same, but their sizes are more consistent. Particles in the 63-125 µm fraction (Fig. 10c) are arranged in a tighter pack and have less variation in shape, suggesting that this fraction consists of more consistent particles. The 0-63 µm fraction (Fig. 10d) exhibits a very fine, homogeneous powder, indicating the most complete heat treatment effect. It is clear from this fraction that, as particle size increases from coarse to fine powder, the smaller particles are more likely to have undergone a more complete and even heat treatment than the larger particles, resulting in greater changes in properties. This analysis suggests that coarser particles require longer heat treatment times to achieve more homogeneous results.

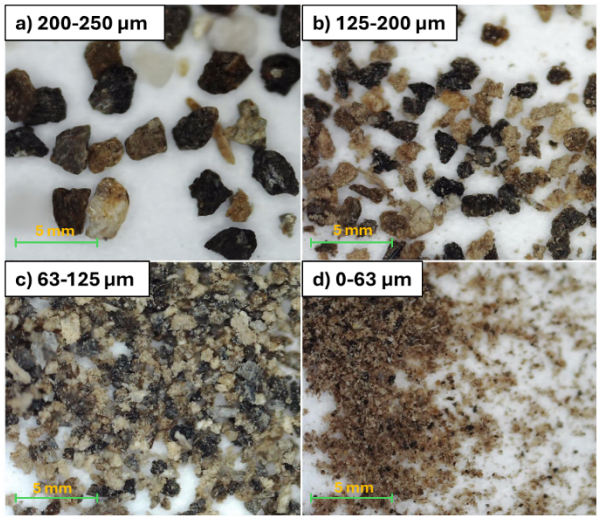

Figure 10. The visual appearance of HTSD at 121 times magnification.

While digital microscopy revealed the general distribution of materials, scanning electron microscopy (SEM) was employed to investigate the finer details of the particle surface textures, porosity, and the complex interface between the wood fibres and cement particles.

The reference residue (Fig. 11) consists of a heterogeneous mixture of elongated wood fibres and irregular hydrated cement particles. As the fraction size decreases, the particles become smaller, and the proportion of cement particles increases, dominating the finer fractions. The wood fibres exhibit progressively more fragmentation and damage in the smaller fractions, although they consistently display rough surfaces due to partial cement coating and processing. At higher magnifications, cement particles are revealed to be conglomerates of smaller particles, with a complex and porous interface with the wood fibres. The material is highly homogeneous and powdery in the finest fraction (<0.063 mm), with individual wood fibres barely distinguishable from the dominant, angular cement particles.

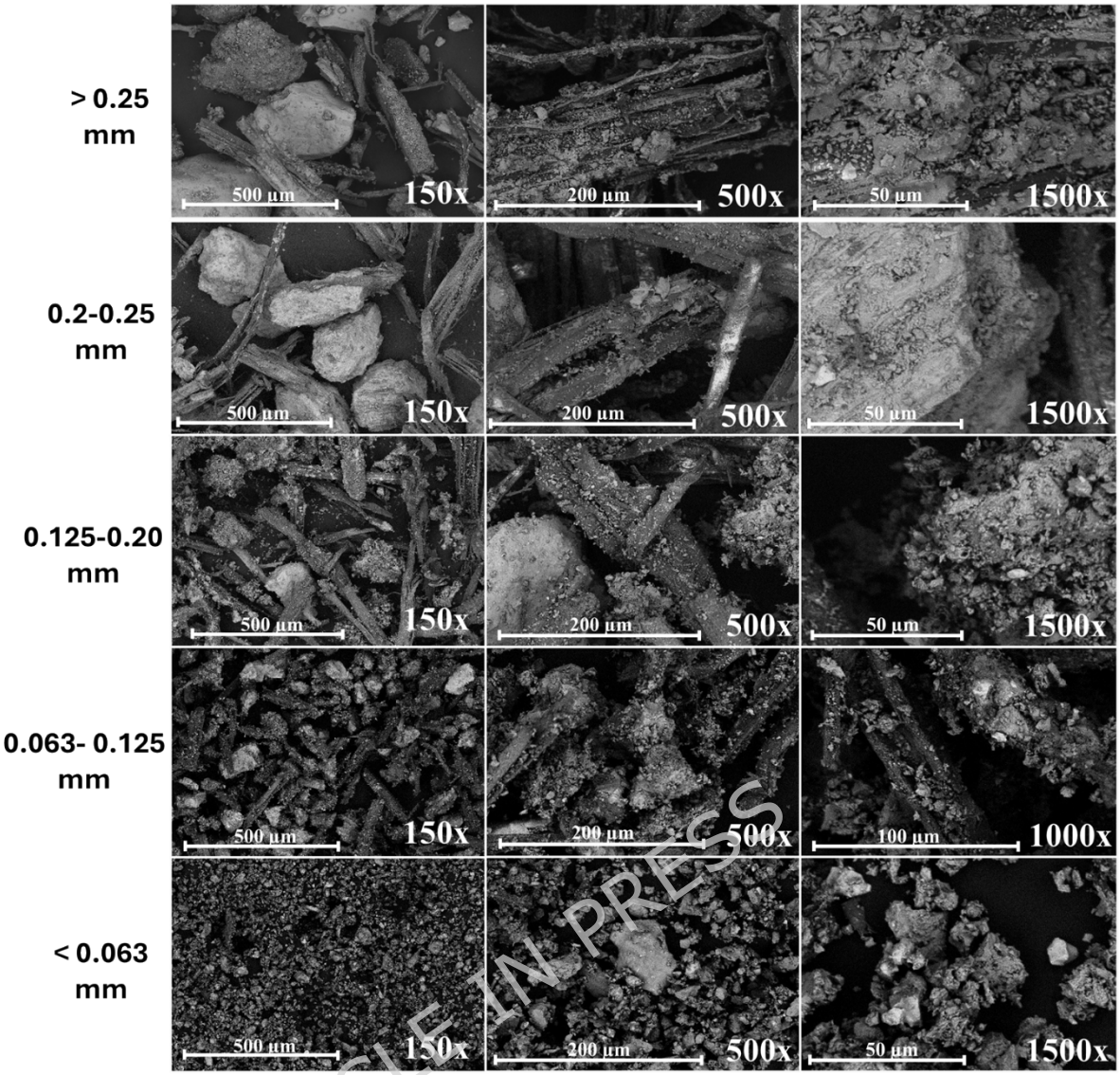

Figure 11. SEM images of different fractions and magnifications of the SD sample.

Following heat treatment at 450 ℃, the organic components, primarily wood fibres, have been largely removed, resulting in a porous inorganic residue. The particles are generally irregular and angular across the different size fractions (Fig. 12), with many exhibiting a porous, granular, or layered texture. At higher magnifications, the microstructure appears highly porous and interconnected, resembling sintered material with partially fused particles. The particles become more uniform in the smaller fractions, and the porosity is more evenly distributed. The finest fraction (<0.063 mm) is a heterogeneous mixture of fine, irregular particles with rough, porous surfaces and lacks distinct fibrous structures. The agglomeration of particles is likely due to partial sintering during heating.

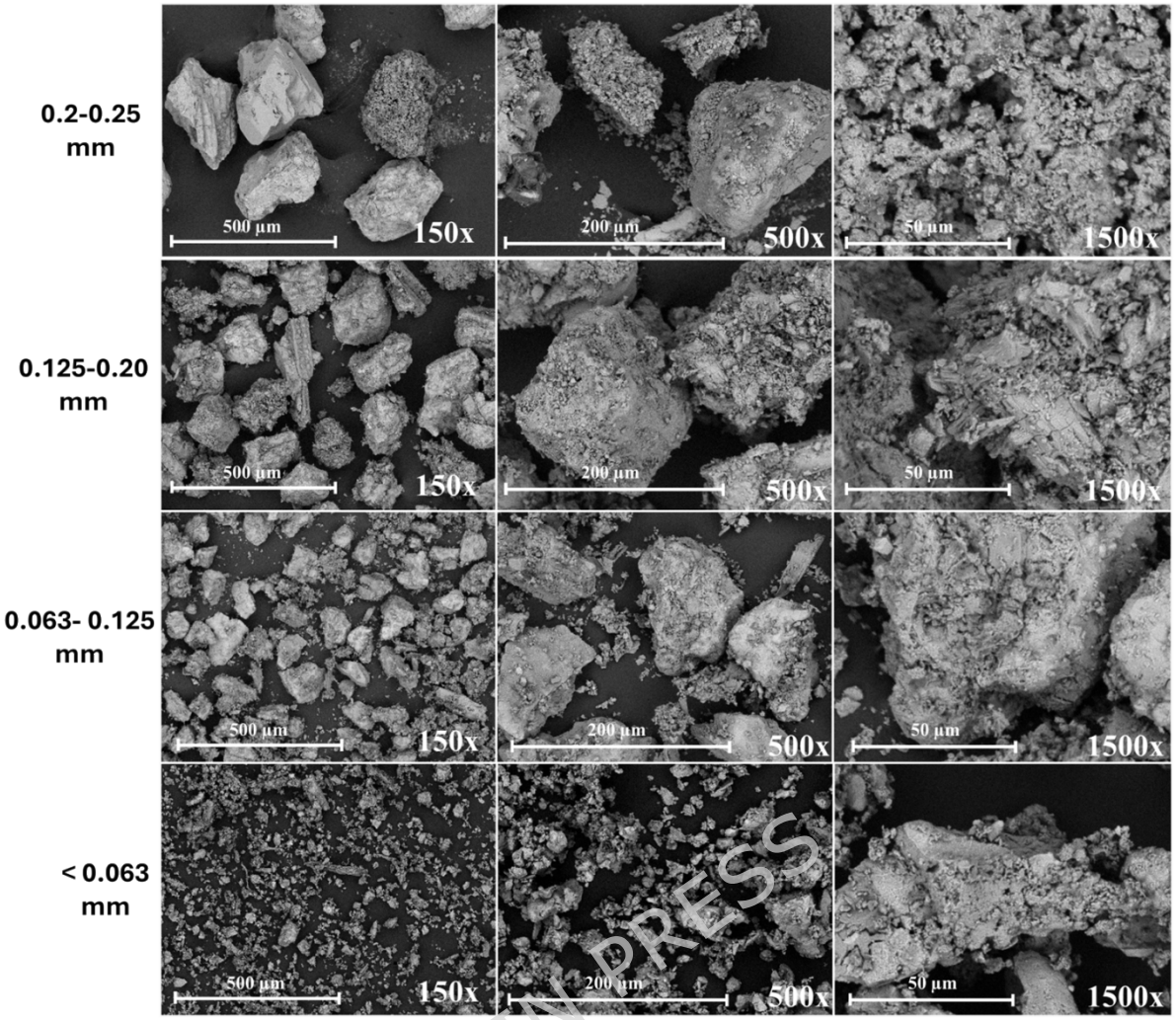

Figure 12. SEM images of different fractions and magnifications of the HTSD sample.

3.1.3. Chemical Composition and Mineralogy

The thermal characteristics of the sanding dust (SD) and heat-treated sanding dust (HTSD) were evaluated using TG/DTA to identify key decomposition and dehydration events (Fig. 13). The SD sample, represented by the blue curve, exhibits a total mass loss of approximately 30 % by 800 ℃.

About 10 % of the mass in the SD sample is lost during the first stage of dehydration (50–150 ℃), which is mostly caused by the evaporation of physically bound water from various sources [65,66]. This includes zeolitic water from aluminate ferrite monosubstituted (AFm) phases in the cement matrix [67], interlayer water from C-S-H gel structures [68], and adsorbed water from wood fibres [66,69]. Ettringites have also been shown to dehydrate at temperatures between 90 and 120 °C [70]. The endothermic nature of this region in the DTA curve confirms the dehydration nature of these processes.

The 150–400 ℃ temperature range shows a slow mass decrease corresponding to wood components' thermal degradation [71–73]. Hemicellulose breaks down first (220–315 ℃) [71,73–75], and then cellulose degradation starts

(315–400 ℃) [71,74,76]. Lignin decomposes progressively over a wide temperature range (200–500 ℃) [66,70,71,73,75,77]. By dehydrating the ettringite (AFt) phases at about 120 ℃ and the AFm phases at 180–200 ℃, the cement phases also contribute to mass loss in this area [78].

At 450 ℃, a characteristic endothermic event with a mass loss step occurs, signifying the dihydroxylation of $Ca(OH)_2$ (Portlandite): $Ca(OH)_2 \rightarrow CaO + H_2O$ [26]. This reaction influences the material's subsequent carbonation behaviour and is essential to cement chemistry [65,66,70–75,77,79–82].

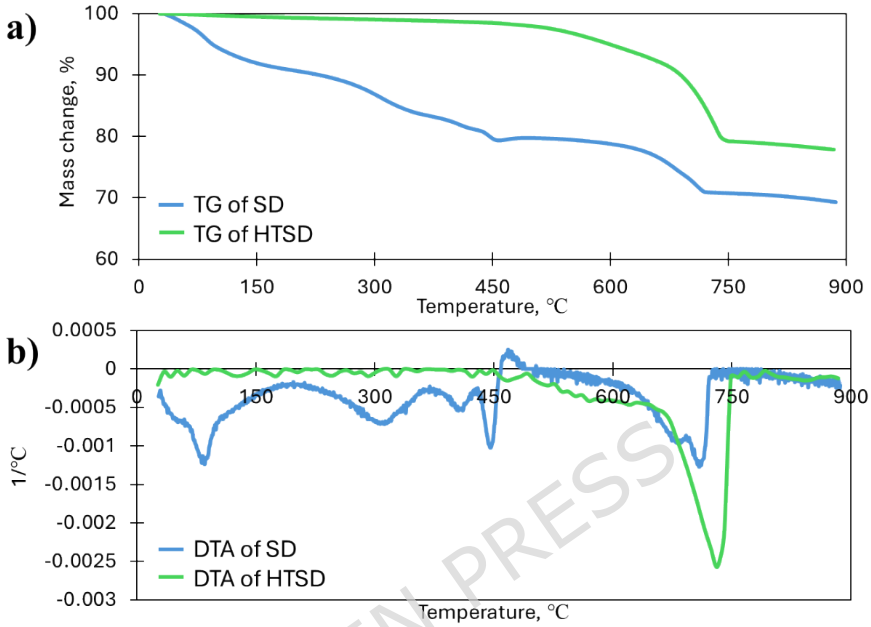

Figure 13. The TG (a) and DTA (b) results of SD and heat-treated sanding dust.

In contrast, the heat-treated sanding dust (HTSD) sample (green curve) exhibits a total mass loss of only 23%. This lower value confirms that the 450 °C treatment successfully removed some organic material and dehydrated the cement phases. The remaining mass loss in this sample is primarily due to the combustion of residual organic matter and the decarbonisation of calcite [65,66,70,72,73,75,77,80–83].

The thermal behavior of the SD and HTSD reveals distinct physicochemical shifts induced by the reactivation process. The slight mass increase observed in the SD sample during initial heating under an air atmosphere is characteristic of the oxidative degradation of lignocellulosic fibers. This phenomenon occurs as oxygen O_2 reacts with the organic matrix to form intermediate oxygenated functional groups (e.g., oxy-cellulose) prior to the primary devolatilization stage [84]. Furthermore, the apparent discrepancy in calcite ($CaCO_3$) content between the two samples is attributed to concentration effects. While XRD analysis confirms that the crystalline structure and absolute quantity of calcite remain stable across both samples, the DTG thermogram records mass loss as a percentage of the total sample weight. Because the heat treatment process removes a significant fraction of volatile organic matter from the SD, the relative

mass proportion of the remaining inorganic phases (including calcite) increases in the HTSD matrix [85]. Thus, the higher DTA peak for HTSD represents a shift in the sample's mass balance rather than a change in mineralogical composition or improper sampling [86].

The oxide composition of waste from the manufacture of wood-wool cement panels changed as it was heated from 0 °C to 450 ℃, as indicated by the XRF data in Table 5. According to the TG/DTA data in Figure 13, the most significant change is an increase in CaO content from 51.11 % to 56.06 %, resulting from the breakdown of calcium-containing compounds, such as calcium carbonates, in hydrated cement. Concurrently, the CO_2 content drops from 25.12 % to 19.72 %, further suggesting that the carbonates are breaking down. SiO_2 gradually rises from 17.02 % to 18.28 %, likely as a result of the oxidation of silicon-containing compounds in wood and the breakdown of calcium silicate hydrates in cement.

Table 5. Oxide distribution of elements.

Sample	SiO_2	Al_2O_3	Fe_2O_3	CaO	MgO	SO_3	Na_2O	K_2O	TiO_2	Mn_2O_3	P_2O_5	Cl	CO_2
SD	17.02	2.49	0.60	51.11	1.70	1.33	0.16	0.16	0.10	0.17	0.03	0.03	25.12
HTSD	18.28	2.72	0.67	56.96	1.79	1.56	0.19	0.19	0.11	0.17	0.03	0.03	19.72

X-ray diffraction (XRD) analysis was performed to identify the crystalline phases of the reference sanding dust (SD) and the heat-treated sanding dust (HTSD), aiming to understand the mineralogical transformations induced by thermal treatment, as shown in Figure 14. The resulting diffractograms reveal changes consistent with the successful reactivation of the cementitious binder.

The reference sanding dust (SD) sample exhibits a phase composition characteristic of a partially hydrated and carbonated cementitious material. The primary hydration products identified were Portlandite ($Ca(OH)_2$), confirmed by its prominent diffraction peaks at 18.1° and 34.1° 2Θ [87], and Ettringite ($Ca_6Al_2(SO_4)_3(OH)_{12}\cdot 25H_2O$), indicated by its signature peak at a low angle of 9.1° 2Θ [88]. The presence of these phases confirms that the cement in the waste material had undergone hydration. A major crystalline phase present is Calcite ($CaCO_3$), identified by its intense peak at 29.4° 2Θ and other peaks at 36.0°, 39.4°, and 48.5° 2Θ [89], which is an expected product of the atmospheric carbonation of Portlandite. Additionally, minor peaks corresponding to Quartz (SiO_2) were identified, with the main peak at 26.6° 2Θ [90], likely originating as a natural impurity from the raw materials of the original cement.

Upon heating to 450 ℃, the material's mineralogy changed. In the HTSD sample's diffractogram, the peaks corresponding to the hydrated phases—Portlandite (18.1°, 34.1° 2Θ) and Ettringite (9.1° 2Θ) — have reduced in intensity to a minimum. This disappearance provides evidence of their thermal decomposition [91,92]. Concurrently, new, sharp diffraction peaks emerge, indicating the formation of Larnite (Ca_2SiO_4), a reactive anhydrous cement clinker phase (also known as Belite, C_2S) [93,94]. The presence of Larnite is

confirmed by distinct peaks at 32.2°, 32.6°, and 41.2° 2Θ, which are not present in the original SD sample [95]. The phases of Calcite and Quartz remain, though their peaks show a marked increase in relative intensity. This is not due to the formation of more material, but rather a concentration effect resulting from the combustion of amorphous organic wood matter and the loss of water, which increases the proportion of crystalline material in the analysed sample [96].

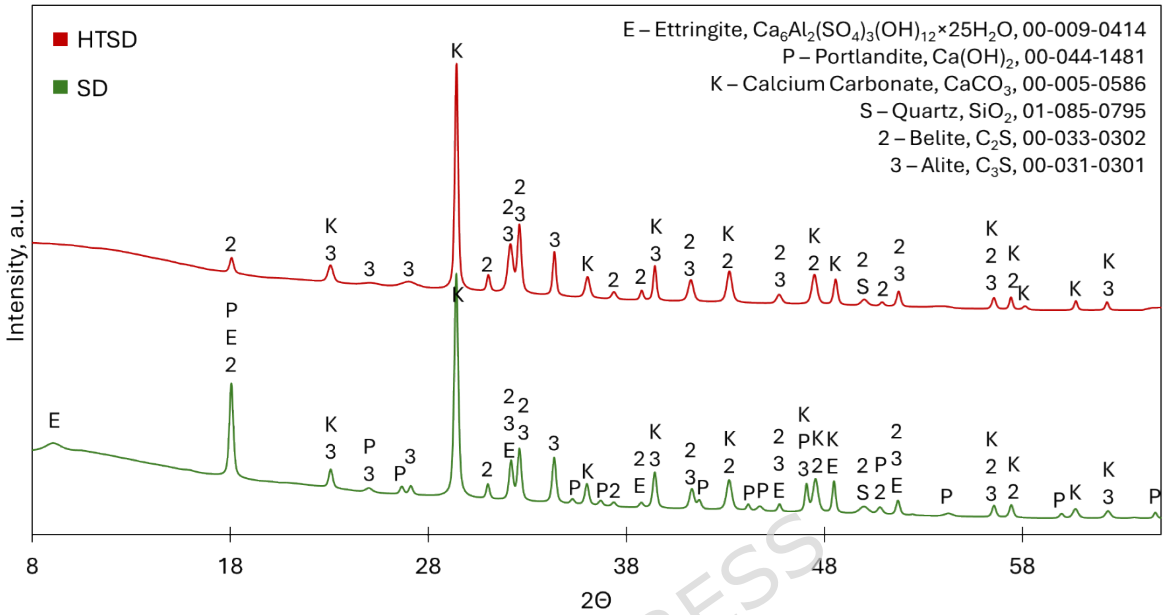

Figure 14. XRD diffractograms of the SD and HTSD Materials.

The initial state of the sanding dust (SD) is established as a stable, hydrated cementitious waste, whose potential 450 °C thermal treatment as a binder is limited by hydration products like Portlandite and Ettringite [97]. The thermal treatment at 450 °C was specifically chosen to target these phases. The intense disappearance of the Portlandite peaks at 18.1° and 34.1° 2Θ is the most critical observation, confirming the successful dihydroxylation of calcium hydroxide into reactive calcium oxide (CaO) and water vapour [98]. This finding aligns perfectly with the thermal analysis data presented in the study, which shows a characteristic mass-loss event for this reaction at 450 °C. Similarly, the decomposition of the AFt phase, Ettringite, contributes to the removal of chemically bound water [99].

However, the most significant indicator of successful reactivation is the formation of Larnite (Belite, C_2S), evidenced by the intensity increase of peaks at 32.2° and 32.6° 2Θ [100]. This demonstrates that the heat treatment did more than dehydrate the material; it induced the recrystallisation of amorphous or poorly crystalline calcium-silicate-hydrate (C-S-H) gels into a stable, anhydrous clinker phase known for its hydraulic properties [101]. Creating this reactive phase is fundamental to restoring the binding capacity of the waste material [102].

3.1.4. Fresh Mortar properties

The setting times for the two samples differ significantly (Table 6). The sanding dust (SD) has a setting start time ranging from 593 to 1168 minutes and finishes setting at approximately 1348 minutes. In contrast, the heat-treated sanding dust (HTSD) starts setting much faster, at just 40 minutes, and completes setting by 180 minutes.

This drastic reduction in setting time for the HTSD sample suggests that the heat-treatment process affects the particle size distribution and enhances the material's reactivity. Smaller particles have a higher surface area-to-volume ratio, which can accelerate chemical reactions and shorten setting times. However, in this case, as the setting times are drastically different, the change may result from the decomposition of wood particles into wood ash particles, which likely contribute to the increased reactivity because they may exhibit pozzolanic properties. These properties enable the particles to react with calcium hydroxide [103] in water, forming compounds that contribute to the material's strength and durability.

Table 6. Setting time compilation of SD and HTSD samples.

Sample	Setting start, min	Setting finish, min
SD	593-1168	~1348
HTSD	40	180

3.1.5. Density and Mechanical Properties

In addition to granulometry, visual appearance, and setting time, density and compressive strength were determined for SD to assess baseline data and compare them with heat-treated SD to assess treatment effects. The compilation of apparent density and compressive strength is shown in Figure 15. Samples were tested on days 2, 7, and 28. Density changed marginally. On day 2, the samples achieved 1390 ± 18 kg/m^3; on day 7, 1397 ± 17 kg/m^{3,} and on day 28, 1384 ± 10 kg/m^3. HTSD achieved a higher density and showed a marginal change: 1605 ± 26 kg/m^3 on day 2, 1647 ± 79 kg/m^3 on day 7, and 1616 ± 5 kg/m^3 on day 28. At 28 days, HTSD has a 16.7 % higher density than SD.

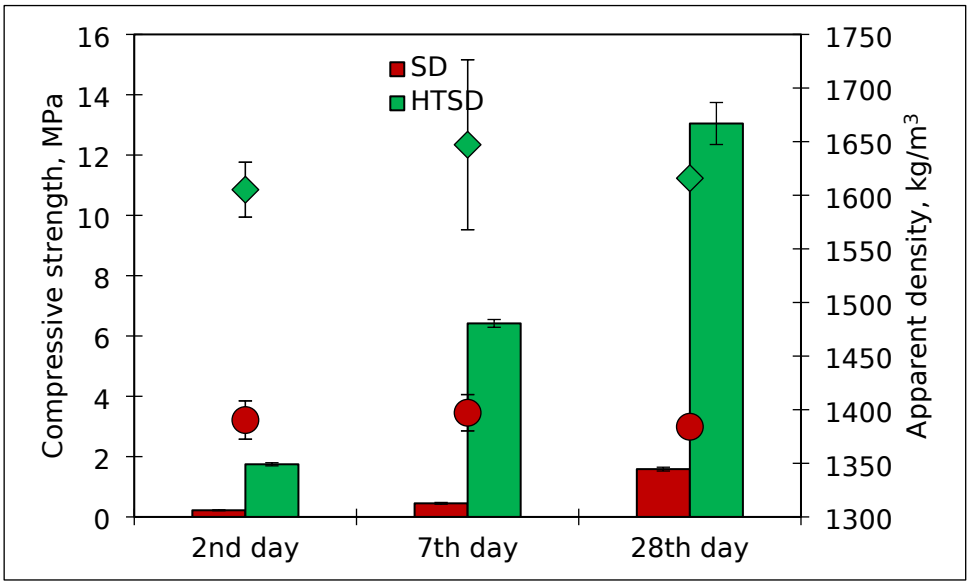

Figure 15. Apparent density and compressive strength compilation of SD and HTSD.

The compressive strength of the SD samples did change beyond the margin of error. According to cement chemistry, this is expected as the compressive strength typically increases with the age of the samples [104]. The SD sample showed relatively low values throughout the measurement days: 0.22 ± 0.02 MPa on the 2nd day, 0.45 ± 0.03 MPa on the 7th day, and 1.59 ± 0.06 MPa on the 28th day. For the HTSD samples, the compressive strength increased to 1.75 ± 0.05 MPa at the 2nd day, 6.42 ± 0.13 MPa at the 7th day, and 13.05 ± 0.70 MPa at the 28th day. The large improvement in compressive strength for the HTSD sample can be attributed to the heat treatment, which altered the microstructure of SD particles and improved bonding and mechanical properties. Overall, the data indicate that heat treatment at 450 ℃ significantly enhances the compressive strength of sanding dust, making it a more robust material than its untreated counterpart.

The mechanical performance of the HTSD (13.05 MPa) aligns with recent findings on the optimal dehydration threshold for recycled cement paste. Recent studies on thermally activated recycled cement waste have reported that dehydration at 450–550 ℃ provides the most efficient balance between rapid hydration kinetics and 28-day strength development, with comparable mortars typically achieving 13.8-17.9 MPa [105,106]. Notably, the HTSD binder in this study significantly surpasses the 28-day strength of 3.99 MPa reported for similar wood-cement manufacturing waste processed through mechanical sifting alone [1], demonstrating that the thermal pathway at 450 ℃ is essential for recovering hydraulic activity.

3.2. Properties of the Biocomposites

The produced binder incorporation into biocomposites was a preliminary demonstration to assess whether this combination is feasible. Biocomposites

were visually assessed to determine whether uniform incorporation of the binder and filler had occurred. The main parameters used to assess the feasibility of the biocomposites were density, thermal conductivity coefficient, and compressive and flexural mechanical strengths.

3.2.1. Visual Analysis

Regarding Fig. 16 and the visual analysis of the developed biocomposites, it is evident that all the above compositions exhibit a uniform appearance, resulting from good mixing and thorough integration of the binder and filler. The top surface is smooth and flat, without cracks or other defects, attesting to high-quality control during preparation. All the samples are coloured the same shade, indicating that the binder-to-filler ratio does not affect their colour. However, similarly formed and sized samples are representative, so differences in properties can be attributed solely to the binder-to-filler (B/F) ratio, without interference from sample size variations. In general, the visual assessment results suggest that variations in the B/F ratio would not significantly affect the visual properties of the samples, indicating that the procedure was adhered to and that the samples were uniform.

Figure 16. Visual appearance of the samples.

3.2.2. Thermal and Physical Properties

Density and thermal conductivity of the developed biocomposites were evaluated. The samples were dried at 45 ℃ until a constant mass was achieved. Material density and thermal conductivity are shown in Figure 17. The standard deviation of all the samples for thermal conductivity data ranges from 0.00003 to 0.00025 W/(m·K). Standard deviation for material density ranges from 23 to 29 kg/m^3.

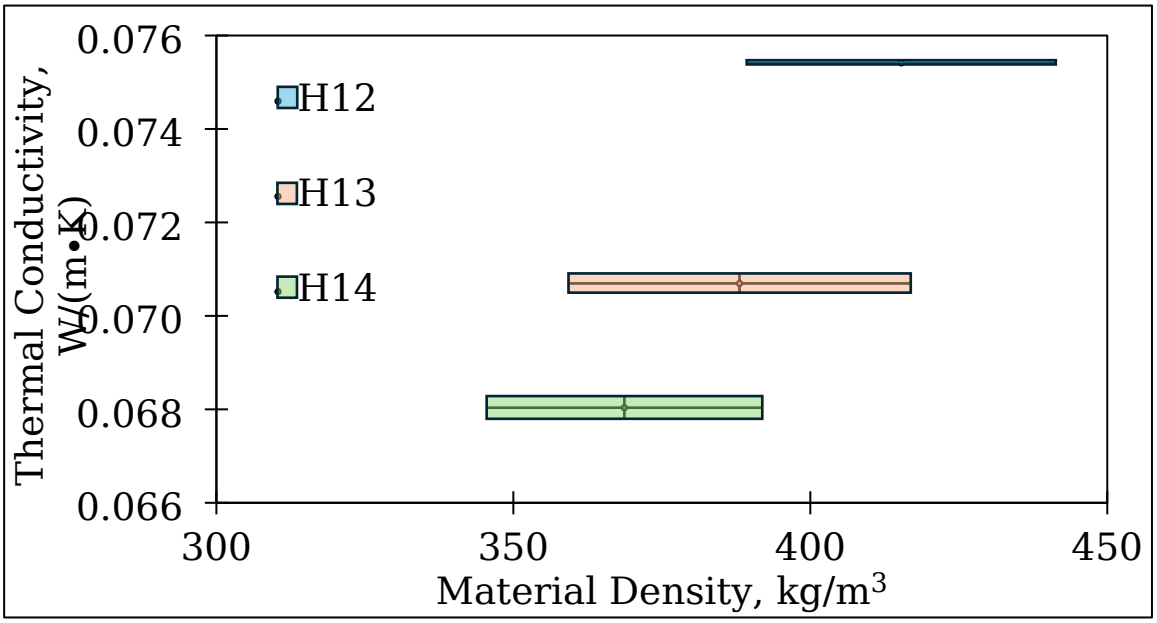

Figure 17. Material density and thermal conductivity compilation.

It is noticeable that increasing the mass fraction of the filler in the composition results in a less dense material. The H14 sample, with a B/F ratio of 1-to-4, had the lowest material density of 369 kg/m^3. The highest material density was achieved for sample H12 (B/F ratio 1-to-2), with a density of 415 kg/m^3. The H13 sample achieved a density of 388 kg/m^3 after drying.

The average thermal conductivity decreased as the filler ratio increased. The highest thermal conductivity was achieved for sample H12, at 0.075 W/(m·K). H13 achieved a thermal conductivity of 0.071 W/(m·K). and the lowest thermal conductivity was achieved for the sample H14, which was 0.068 W/(m•K).

3.2.3. Mechanical Properties

In Table 7, mechanical properties are compiled. Mechanical properties include flexural and compressive strength, which are tested in different directions. Table 6 shows that compressive strength has been tested at 10 and 20 % compression rates based on the sample's height, and the samples have been tested in two directions – forming direction and perpendicular to forming direction.

Table 7. Compressive and flexural strength compilation of the samples.

Sample	Testing direction	Average compressive strength 10 % (perpendicular to forming direction - critical strength), kPa	Average compressive strength 20 %, kPa	Flexural strength. kPa
H12	Forming direction	175 ± 10	184 ± 14	100 ± 28

	Perpendicular to the forming direction	97 ± 13		87 ± 42
H13	Forming direction	75 ± 10	119 ± 15	31 ± 1
	Perpendicular to the forming direction	27 ± 2		64 ± 21
H14	Forming direction	26 ± 8	62 ± 5	38 ± 8
	Perpendicular to the forming direction	61 ± 7		38 ± 19

The analysis of the compressive and flexural strengths of samples H12, H13, and H14 reveals distinct variations in their mechanical properties. Sample H12 demonstrates the highest compressive strength in the forming direction, with 175 ± 10 kPa at 10 % deformation and 184 ± 14 kPa at 20 % deformation, alongside a notable flexural strength of 100 ± 28 kPa. In contrast, the perpendicular direction shows lower compressive strength (97 ± 13 kPa at 10 % deformation) and flexural strength (87 ± 42 kPa). The higher strength compared to other samples can be attributed to a higher binder content, which leads to stronger bonding with the filler. Sample H13 exhibits lower strengths, with compressive strengths of 75 ± 10 kPa and 119 ± 15 kPa in the forming direction (10 % and 20 % compression, respectively) and 27 ± 2 kPa in the perpendicular direction at 10 % deformation. Flexural strength for sample H13 in the forming direction was 31 ± 1 kPa, and in the perpendicular direction to the forming direction, 64 ± 21 kPa. Sample H14 presents higher compressive strength perpendicular to the forming direction at 10 % deformation (61 ± 7 kPa) compared to the forming direction (26 ± 8 kPa). However, this trend reverses at 20 % deformation, with the forming direction showing 62 ± 5 kPa. The flexural strength for H14 is moderate at 38 ± 8 kPa. The difference in the testing directions can be attributed to the alignment of wood-wool fibres during the forming process. These findings highlight the influence of testing direction on the mechanical properties of the samples, with significant implications for their potential applications. Fig. 18 has been compiled to include all mechanical properties for better data visualization.

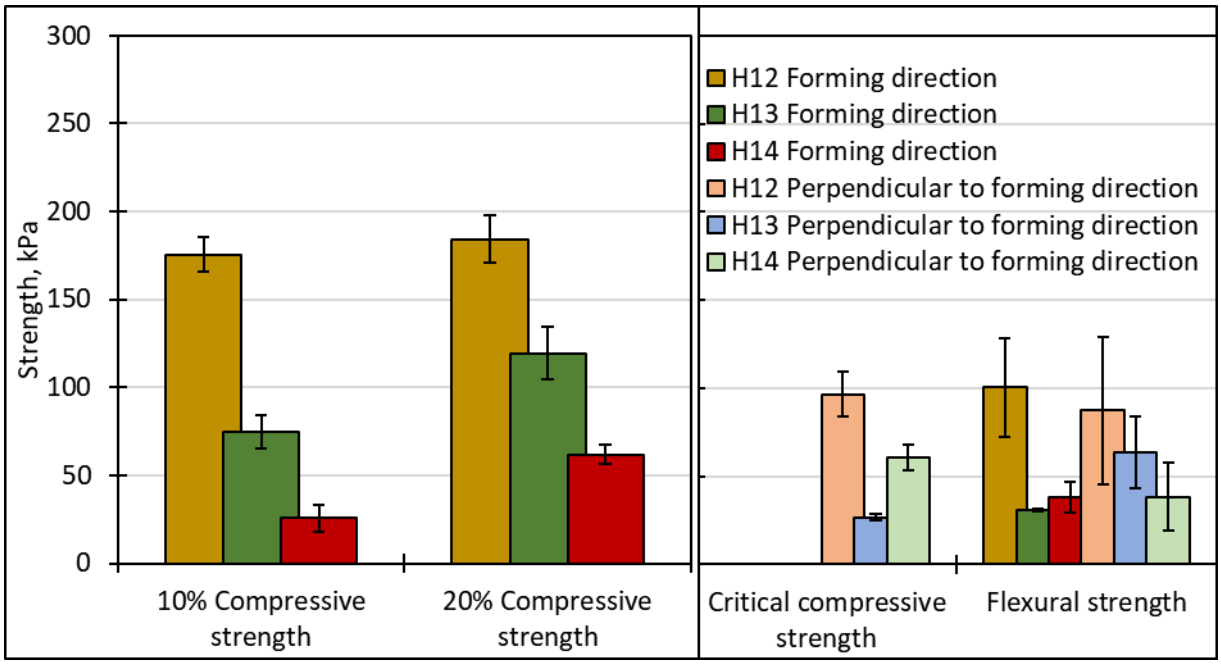

Figure 18. Mechanical property compilation of the biocomposites.

The compressive strength of the HTSD-based biocomposites (26-184 kPa) reflects their intended application as functional, non-structural thermal insulation. These results are consistent with the mechanical performance of other innovative circular binder systems, such as ternary bio-composites developed through accelerated carbonation, which typically target similar low-density ranges for sustainable construction [33]. The peak strength achieved (184 kPa) aligns with findings from comparable studies on thermoactivated recycled cement, where dehydration at 450–550 ℃ recovers sufficient hydraulic capacity to stabilize porous structures without requiring the energy intensity of full re-clinkering [105,106].

3.3. Life Cycle Assessment

The Life Cycle Assessment (LCA) revealed significant variations in global warming potential. The impact on global warming was calculated per 1 m^3 of the binder. The thermal treatment at 450 ℃ resulted in 387 kg CO_2 eq. per 1 m^3 of binder. Conventional CEM II/A-LL 42.5 N cement showed the highest impact of 1040 kg CO_2 eq. That represents a 63 % decrease in CO_2 eq emissions per 1 m^3 of binder.

Table 8 presents the mix design and properties of the proposed biocomposites, which exhibit comparable compressive strengths, enabling comparison of their environmental impacts.

Table 8. Mix design and properties of the interpolated biocomposites with representative compressive strength.

Binder type	Name	Binder, kg/m^3	Water for	Filler, kg/m^3	Compressive strength 10 %, MPa	Thermal conductivity, W/(m·K)	Density, kg/m^3	Thic a U=

			Binder, kg/m^3					W/(m
HTSD	HTSD(0.05)	80	48	274	0.05	0.069	378	0.
	HTSD(0.15)	117	70	256	0.15	0.074	408	0.
	HTSD(0.5)	247	148	193	0.5	0.091	514	0.
CEM II/A-LL 42.5 N	CEM(0.05)	5	20	301	0.05	0.068	361	0.
	CEM(0.15)	79	31	299	0.15	0.072	394	0.
	CEM(0.5)	176	70	294	0.5	0.087	506	0.

Following the environmental impact assessment of binders, evaluating the life cycle performance of the resulting biocomposites is crucial, as their practical applications ultimately determine their environmental value. Overall emissions are shown in Figure 19. The total emissions per kg CO_2 eq. per U-value 0.18 W(m^{2}K) range from 10 kg CO_2 eq. for HTSD(0.05) to 53 kg CO_2 eq. for CEM(0.5), demonstrating a clear correlation between compressive strength and environmental impact.

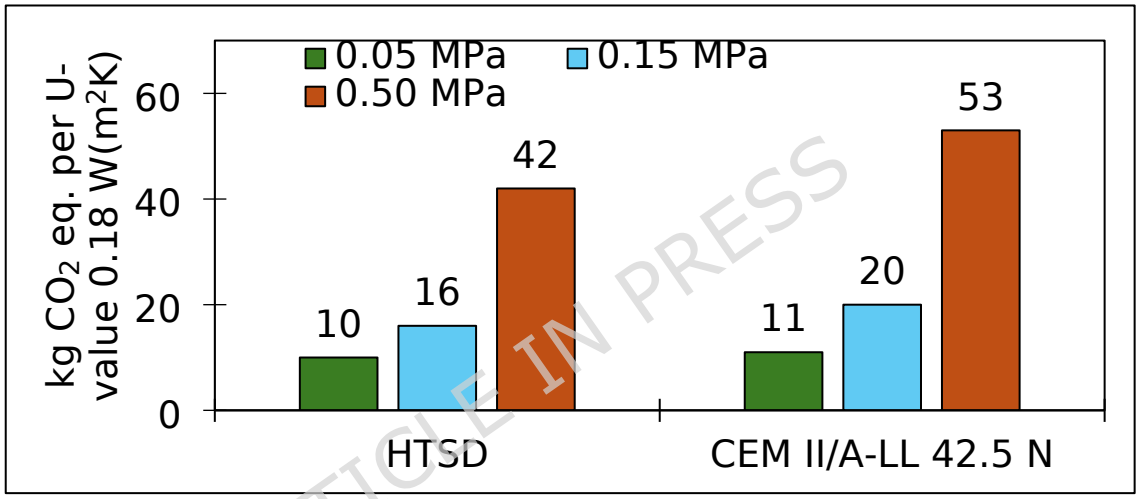

Figure 19. Overall emissions per kg CO_2 eq. per U-value 0.18 W(m^{2}K) of the biocomposites.

Biocomposites with thermally treated binder at 450 ℃ (HTSD) achieved emissions ranging from 10 to 42 kg CO_2 eq. per U-value 0.18 W(m^{2}K). However, their environmental impact is primarily attributed to heating energy requirements. The achieved emissions across all compressive strength classes for the HTSD biocomposites are lower than those of their alternative CEM II constituent, indicating that the proposed thermal treatment for SD is promising for sustainable building materials.

4. CONCLUSIONS

This study successfully demonstrated the viability of transforming sanding dust (SD), a by-product of wood-wool cement panel manufacturing, into a reactive cementitious binder via targeted thermal treatment. The subsequent application of this reactivated binder in the fabrication of new bio-based building

materials was evaluated, confirming the potential of this circular economy approach to create value-added products from industrial residues.

The investigation into the properties of the heat-treated sanding dust (HTSD) as a standalone binder yielded several key findings:

- Heat treatment at 450 °C effectively refined the binder's physical properties, reducing the average particle size by 35% (from 29.21 µm to 19.11 µm) and increasing the Blaine surface area from 2420 to 2996 cm^2/g. XRD and TGA results confirmed the intended mineralogical changes, showing a decomposition of hydrated phases like Portlandite (at 18.1° and 34.1° 2Θ) and Ettringite (at 9.1° 2Θ);
- The most significant outcome was the formation of Larnite (C_2S), a reactive anhydrous clinker phase, confirmed by new XRD peaks at 32.2°, 32.6°, and 41.2° 2Θ. This demonstrated a successful reactivation beyond simple dehydration;
- The reactivated binder (HTSD) performed better than the original sanding dust. The setting start time was drastically reduced from over 9 hours to just 40 minutes;
- The 28-day compressive strength saw a remarkable eight-fold increase from 1.59 MPa to 13.05 MPa, confirming its restored binding capacity;
- The Life Cycle Assessment confirmed the environmental aspect of the reactivated binder, which achieved a 63 % reduction in global warming potential compared to conventional CEM II (387 vs. 1040 kg CO_2 eq./m^3).

The successful development of the reactivated binder enabled its use as a binder in new lightweight biocomposites, with production-line waste as a filler. The analysis of these biocomposites led to the following conclusions:

- The B/F ratio directly influenced the material properties. Increasing the proportion of filler (2 to 4) consistently lowered the material's density (from 415 kg/m^3 to 369 kg/m^3) and, consequently, its thermal conductivity (from 0.075 W/(m·K) down to 0.068 W/(m·K)), highlighting its potential as an effective insulation material;
- Biocomposites with a B/F ratio of 1-to-2 (H12) show higher compressive strength in the forming direction compared to the perpendicular direction (175 and 97 kPa). Biocomposites with a B/F ratio of 1-to-3 (H13) also exhibit higher compressive strength in the forming direction (75 and 27 kPa), though the values are much lower than those of H12. The Biocomposites with a B/F ratio of 1-to-4 (H14) achieved similar strengths at 20 % compression in the forming direction and at the perpendicular direction – 62 and 61 kPa, respectively;
- The biocomposites displayed anisotropic mechanical properties, with strengths generally higher when tested in the forming direction compared to the perpendicular direction, a critical consideration for structural applications;

- The biocomposites produced with the heat-treated binder demonstrated consistently lower total emissions (10-42 kg CO_2 eq. per functional unit) across all compressive strength classes, validating the thermal reactivation method as a sustainable pathway for producing low-carbon building materials.

This research addresses a critical need within the construction industry to mitigate its significant environmental impact, particularly in terms of raw material consumption and waste generation. This study presents a tangible pathway toward a circular manufacturing model by establishing a validated method for upcycling wood-wool cement panel residues. It is projected that 174 million m^2 of wood-wool cement panels will be produced worldwide, with 25 % coming from Europe [107]. In the long term, implementing such processes at an industrial scale can substantially reduce reliance on landfills, decrease demand for virgin cement production, and create sustainable, low-carbon building materials. This work provides a robust proof of concept, encouraging further development of reactivation technologies to transform industrial waste streams into valuable resources and thereby contribute to a more sustainable, resource-efficient construction sector. By providing a complete 'waste-to-product' pathway for this specific industrial residue, this study offers a validated model that can be adapted for similar underutilised cementitious by-products globally.

Author Contributions: Conceptualization, P.P.A.; methodology, P.P.A. and L.P.; validation, P.P.A.; D.B.; L.V.; X.Z. M.S.; formal analysis, P.P.A.; investigation, P.P.A. and L.P.; resources, P.P.A. and D.B.; data curation, P.P.A.; writing—original draft preparation, P.P.A. and L.V.; writing—review and editing, P.P.A.; X.Z.; L.V.; D.B.; M.S.; visualisation, P.P.A. and L.V.; supervision, L.V.; project administration, P.P.A.; funding acquisition, P.P.A. and D.B. All authors have read and agreed to the published version of the manuscript.

Funding: This activity/work has been supported by the EU Recovery and Resilience Facility within the Project No 5.2.1.1.i.0/2/24/I/CFLA/003 "Implementation of consolidation and management changes at Riga Technical University, Liepaja University, Rezekne Academy of Technology, Latvian Maritime Academy and Liepaja Maritime College for the progress towards excellence in higher education, science and innovation" academic career doctoral grant (ID 1003).

Declarations

Competing Interest: NO

Dual Publication: NO

Third Party Material: NO

Data Availability: YES. The datasets generated and analysed during the current study are not publicly available because the data are sensitive to the

manufacturing company, but are available from the corresponding author upon reasonable request.

Acknowledgments: The authors would like to thank Cewood Ltd. for supplying the materials used for the experiments. This article is part of the first author's doctoral thesis, “Recycling of Wood-Cement Manufacturing Waste into Innovative Building Materials,” which has been defended on 19th September 2025 [26].

Conflicts of Interest: The authors declare no conflicts of interest.

REFERENCES

1. Argalis, P.P.; Sinka, M.; Bajare, D. Recycling of Cement–Wood Board Production Waste into a Low-Strength Cementitious Binder. *Recycling* **2022**, *7*, 76, doi:10.3390/recycling7050076.
2. Bumanis, G.; Argalis, P.P.; Sinka, M.; Korjakins, A.; Bajare, D. The Use of Recycled Cement-Bonded Particle Board Waste in the Development of Lightweight Biocomposites. *Materials* **2024**, *17*, 5890, doi:10.3390/ma17235890.
3. Suarez-Riera, D.; Restuccia, L.; Falliano, D.; Ferro, G.A.; Tuliani, J.M.; Pavese, M.; Lavagna, L. An Overview of Methods to Enhance the Environmental Performance of Cement-Based Materials. *Infrastructures 2024, Vol. 9, Page 94* **2024**, *9*, 94, doi:10.3390/INFRASTRUCTURES9060094.
4. Kaptan, K.; Cunha, S.; Aguiar, J. A Review of the Utilization of Recycled Powder from Concrete Waste as a Cement Partial Replacement in Cement-Based Materials: Fundamental Properties and Activation Methods. *Applied Sciences 2024, Vol. 14, Page 9775* **2024**, *14*, 9775, doi:10.3390/APP14219775.
5. Schneider, M.; Romer, M.; Tschudin, M.; Bolio, H. Sustainable Cement Production—Present and Future. *Cem. Concr. Res.* **2011**, *41*, 642–650, doi:10.1016/J.CEMCONRES.2011.03.019.
6. Barbhuiya, S.; Kanavaris, F.; Das, B.B.; Idrees, M. Decarbonising Cement and Concrete Production: Strategies, Challenges and Pathways for Sustainable Development. *Journal of Building Engineering* **2024**, *86*, doi:10.1016/J.JOBE.2024.108861.
7. IEA *Breakthrough Agenda Report 2023*; Paris, 2023;
8. GlobalABC *Global Status Report*; 2023;
9. Gibbs, M.J.; Soyka, P.; Connely, D. CO 2 Emissions from Cement Production. In *Good Practice Guidance and Uncertainty Management in National Greenhouse Gas Inventories*; 2021; pp. 175–182.
10. Ramsden, K. *Cement and Concrete: The Environmental Impact*; 2020;

11. Dharmadhikari, S. Review of Treatment Methods for Enhancing Recycled Concrete Aggregates Properties. *Int. J. Res. Appl. Sci. Eng. Technol.* **2024**, *12*, 2812–2820, doi:10.22214/IJRASET.2024.59486.
12. Pawluczuk, E.; Kalinowska-Wichrowska, K.; Bołtryk, M.; Jiménez, J.R.; Fernández, J.M. The Influence of Heat and Mechanical Treatment of Concrete Rubble on the Properties of Recycled Aggregate Concrete. *Materials 2019, Vol. 12, Page 367* **2019**, *12*, 367, doi:10.3390/MA12030367.
13. Sui, Y.; Ou, C.; Liu, S.; Zhang, J.; Tian, Q. Study on Properties of Waste Concrete Powder by Thermal Treatment and Application in Mortar. *Applied Sciences 2020, Vol. 10, Page 998* **2020**, *10*, 998, doi:10.3390/APP10030998.
14. Vengadesh Marshall Raman, J.; Ramasamy, V. Various Treatment Techniques Involved to Enhance the Recycled Coarse Aggregate in Concrete: A Review. *Mater. Today Proc.* **2020**, *45*, 6356–6363, doi:10.1016/J.MATPR.2020.10.935.
15. Pawluczuk, E.; Kalinowska-Wichrowska, K.; Bołtryk, M.; Jiménez, J.R.; Fernández, J.M. The Influence of Heat and Mechanical Treatment of Concrete Rubble on the Properties of Recycled Aggregate Concrete. *Materials* **2019**, *12*, doi:10.3390/MA12030367.
16. Shima, H.; Tateyashiki, H.; Matsuhashi, R.; Yoshida, Y. *An Advanced Concrete Recycling Technology and Its Applicability Assessment through Input-Output Analysis*; 2005; Vol. 3;.
17. Semugaza, G.; Mielke, T.; Castillo, M.E.; Gierth, A.Z.; Tam, J.X.; Nawrath, S.; Lupascu, D.C. Reactivation of Hydrated Cement Powder by Thermal Treatment for Partial Replacement of Ordinary Portland Cement. *Materials and Structures/Materiaux et Constructions* **2023**, *56*, doi:10.1617/s11527-023-02133-9.
18. Semugaza, G. Reactivation of Hydrated Cement and Recycled Concrete Powders by Thermal Treatment for Partial Replacement of Virgin Cement, Von der Fakultät für IngenieurwissenschaftenAbteilung Bauwissenschaften: Essen, 2024.
19. Carriço, A.; Bogas, J.A.; Guedes, M. Thermoactivated Cementitious Materials – A Review. *Constr. Build. Mater.* **2020**, *250*, 118873, doi:10.1016/J.CONBUILDMAT.2020.118873.
20. Moreno-Juez, J.; Vegas, I.J.; Frías Rojas, M.; Vigil de la Villa, R.; Guede-Vázquez, E. Laboratory-Scale Study and Semi-Industrial Validation of Viability of Inorganic CDW Fine Fractions as SCMs in Blended Cements. *Constr. Build. Mater.* **2021**, *271*, 121823, doi:10.1016/J.CONBUILDMAT.2020.121823.
21. Choi, H.; Lim, M.; Choi, H.; Kitagaki, R.; Noguchi, T.; Choi, H.; Lim, M.; Choi, H.; Kitagaki, R.; Noguchi, T. Using Microwave Heating to Completely

Recycle Concrete. *J. Environ. Prot. (Irvine,. Calif).* **2014**, *5*, 583–596, doi:10.4236/JEP.2014.57060.

22. Gholizadeh-Vayghan, A.; Meza Hernandez, G.; Kingne, F.K.; Gu, J.; Dilissen, N.; El Kadi, M.; Tysmans, T.; Vleugels, J.; Rahier, H.; Snellings, R. Thermal Reactivation of Hydrated Cement Paste: Properties and Impact on Cement Hydration. *Materials 2024, Vol. 17, Page 2659* **2024**, *17*, 2659, doi:10.3390/MA17112659.
23. Tantawy, M.A. Effect of High Temperatures on the Microstructure of Cement Paste. *Journal of Materials Science and Chemical Engineering* **2017**, *05*, 33–48, doi:10.4236/MSCE.2017.511004.
24. BAROT, R.S.; Ayar, M.; Beravala, D.H.S. Energy Efficient and Sustainable Design and Development of Muffle Furnace for Melting Alloys. *SSRN Electronic Journal* **2019**, doi:10.2139/SSRN.3462641.
25. Kamal, I.; Abed, A.A. The Impact of High Temperatures on the Strength of Recycled Aggregate Concrete. *E3S Web of Conferences* **2025**, *621*, doi:10.1051/e3sconf/202562101009.
26. P. Ārgalis, P. Recycling of Wood-Cement Manufacturing Waste into Innovative Building Materials. Doctoral Thesis, Riga Technical University: Latvia, Riga, 2025.
27. Rahimpour, H.; Esmaeili, J. Characterization, Mechanical Strength, Rheological Properties and Life Cycle Assessment of Fully Recycled Concrete through Geopolymer Technology. *Scientific Reports 2025 15:1* **2025**, *15*, 9424-, doi:10.1038/s41598-025-92307-y.
28. Rahimpour, H.; Amini, A.B.; Sharifi, F.; Fahmi, A.; Zinatloo-Ajabshir, S. Facile Fabrication of Next-Generation Sustainable Brick and Mortar through Geopolymerization of Construction Debris. *Scientific Reports 2024 14:1* **2024**, *14*, 10914-, doi:10.1038/s41598-024-61688-x.
29. Fahmi, A.; Zavaragh, S.R.; Hanafi, M.R.; Rahimpour, H.; Zinatloo-Ajabshir, S.; Asghari, A. Facile Preparation, Characterization, and Investigation of Mechanical Strength of Starchy NaCl-Binder as a Lightweight Construction Material. *Sci. Rep.* **2023**, *13*, 108060, doi:10.1038/s41598-023-46536-8.
30. Hanafi, M.R.; Rahimpour, H.; Gholampour, A.; Ghaffar, S.H.; Moodi, F.; Zarrabi, H.; Fahmi, A. Geopolymer from Sand Washing Waste: Mechanical, Rheological, and Sustainability Perspectives. *Results in Engineering* **2025**, *28*, 108060, doi:10.1016/j.rineng.2025.108060.
31. Rahimpour, H.; Ghiasi, V.; Fahmi, A.; Marabi, Y. Geopolymer vs Ordinary Portland Cement: Review of the 3-d Printing of Concrete. *Applied Engineering and Technology* **2023**, *2*, 133–152, doi:10.31763/aet.v2i2.1010.
32. Hanafi, M.R.; Rahimpour, H.; Golsefidi, Z.B.; Zinatloo-Ajabshir, S.; Mollaei, S.; Moodi, F.; Zarrabi, H.; Fahmi, A. Upcycling Autoclaved Aerated Concrete into Sustainable and Energy-Efficient Geopolymers with

Improved Structural Attributes. *Energy Nexus* **2026**, *21*, 100685, doi:10.1016/j.nexus.2026.100685.

33. Rahmani, H.; Rahimpour, H.; Hanafi, M.R.; Algirdas, A.; Zinatloo-Ajabshir, S. Low-Carbon Ternary Binder Bio-Composites via Accelerated Carbonation for Circular Construction. *Developments in the Built Environment* **2026**, *25*, 100874, doi:10.1016/j.dibe.2026.100874.
34. Dunant, C.F.; Joseph, S.; Prajapati, R.; Allwood, J.M. Electric Recycling of Portland Cement at Scale. *Nature 2024 629:8014* **2024**, *629*, 1055–1061, doi:10.1038/s41586-024-07338-8.
35. Chinedu Alex Ezeigweneme; Chibuike Daraojimba; Olawe Alaba Tula; Abimbola Oluwatoyin Adegbite; Joachim Osheyor Gidiagba A Review of Technological Innovations and Environmental Impact Mitigation. *World Journal of Advanced Research and Reviews* **2024**, *21*, 075–082, doi:10.30574/WJARR.2024.21.1.2687.
36. Gholizadeh-Vayghan, A.; Meza Hernandez, G.; Kingne, F.K.; Gu, J.; Dilissen, N.; El Kadi, M.; Tysmans, T.; Vleugels, J.; Rahier, H.; Snellings, R. Thermal Reactivation of Hydrated Cement Paste: Properties and Impact on Cement Hydration. *Materials 2024, Vol. 17, Page 2659* **2024**, *17*, 2659, doi:10.3390/MA17112659.
37. Sui, Y.; Ou, C.; Liu, S.; Zhang, J.; Tian, Q. Study on Properties of Waste Concrete Powder by Thermal Treatment and Application in Mortar. *Applied Sciences 2020, Vol. 10, Page 998* **2020**, *10*, 998, doi:10.3390/APP10030998.
38. ÇELEKLİ, A.; ZARİÇ, Ö.E. From Emissions to Environmental Impact: Understanding the Carbon Footprint. *International Journal of Environment and Geoinformatics* **2023**, *10*, 146–156, doi:10.30897/IJEGEO.1383311.
39. Klee, H. *World Business Council for Sustainable Development The Cement Sustainability Initiative Recycling Concrete*; 2024;
40. Ning, Z. *Thermal Treatment of Recycled Concrete Fines*;
41. Argalis, P.P.; Sinka, M.; Andzs, M.; Korjakins, A.; Bajare, D. Development of New Bio-Based Building Materials by Utilising Manufacturing Waste. *Environmental and Climate Technologies* **2024**, *28*, 58–70, doi:10.2478/rtuect-2024-0006.
42. Cement Board Market - Share & Size Available online: https://www.mordorintelligence.com/industry-reports/cement-board-market (accessed on 25 November 2025).
43. Bumanis, G.; Argalis, P.P.; Sinka, M.; Korjakins, A.; Bajare, D. The Use of Recycled Cement-Bonded Particle Board Waste in the Development of Lightweight Biocomposites. *Materials* **2024**, *17*, 5890, doi:10.3390/ma17235890.
44. Argalis, P.P.; Puzule, L.; Sinka, M.; Bajare, D. Transforming Cement-Wood Fiber Industrial Byproducts into Hybrid Binder. In *Bio-Based Building*

Materials - Proceedings of ICBBM 2025; Springer Nature, 2025; pp. 738–751.
45. Statements, B.; Size, T. Standard Test Method for Sieve Analysis of Fine and Coarse Aggregates. *Annual Book of ASTM Standards* **2011**, 5–9.
46. Jig, F.T.; Oven, G.C.; Scraper, P. Standard Test Method for Slump of Sealants 1. **2014**, *i*, 1–4, doi:10.1520/C0143.
47. epd-norge *Environmental Product Declaration of Schwenk CEM II/B-M (P-LL) 42.5 N*; 2023;
48. Lasvaux, S. Study of a Simplified Model for the Life Cycle Assessment of Buildings, Paris, 2010.
49. Aggarwal, R.; Gustavsson, M.; Peters, G.; Molander, S. Extrapolation Factors for Calculating Ecotoxicity Effects in LCA. *The International Journal of Life Cycle Assessment 2024 30:1* **2024**, *30*, 134–150, doi:10.1007/S11367-024-02357-Z.
50. Cucurachi, S.; Steubing, B.; Siebler, F.; Navarre, N.; Caldeira, C.; Sala, S. Prospective LCA Methodology for Novel and Emerging Technologies for Bio-Based Products Available online: https://op.europa.eu/en/publication-detail/-/publication/778841cc-6a36-11ed-b14f-01aa75ed71a1/language-en (accessed on 1 April 2026).
51. Hodkova, J.; Lasvaux, S. Guidelines for the Use of Existing Life Cycle Assessment Data on Building Materials as Generic Data for a National Context. In Proceedings of the RILEM laboratories publications; 2012.
52. Saad, M.; Zhang, Y.; Jia, J.; Tian, J. Decision Tree-Based Approach to Extrapolate Life Cycle Inventory Data of Manufacturing Processes. *J. Environ. Manage.* **2024**, *360*, 121152, doi:10.1016/J.JENVMAN.2024.121152.
53. van der Hulst, M.K.; Hauck, M.; Hoeks, S.; van Zelm, R.; Huijbregts, M.A.J. Learning Curves in Prospective Life Cycle Assessment. *Environ. Sci. Technol.* **2025**, *59*, 16501, doi:10.1021/ACS.EST.5C03870.
54. Dawel, L.; Schmedes, F.; Penaherrera Vaca, F.A.; Pehlken, A. Application of Matrix Completion Techniques on LCA Data for Different Recycling Scenarios for Parts of Professional Data Centers. *Procedia CIRP* **2025**, *135*, 888–893, doi:10.1016/J.PROCIR.2024.12.088.
55. Galvez-Martos, J.L.; Schoenberger, H. An Analysis of the Use of Life Cycle Assessment for Waste Co-Incineration in Cement Kilns. *Resour. Conserv. Recycl.* **2014**, *86*, 118–131, doi:10.1016/J.RESCONREC.2014.02.009.
56. Gopalraj, S.K.; Deviatkin, I.; Horttanainen, M.; Kärki, T. Life Cycle Assessment of a Thermal Recycling Process as an Alternative to Existing CFRP and GFRP Composite Wastes Management Options. *Polymers 2021, Vol. 13, Page 4430* **2021**, *13*, 4430, doi:10.3390/POLYM13244430.
57. Pedreño-Rojas, M.A.; Fořt, J.; Černý, R.; Rubio-de-Hita, P. Life Cycle Assessment of Natural and Recycled Gypsum Production in the Spanish

Context. *J. Clean. Prod.* **2020**, *253*, 120056, doi:10.1016/J.JCLEPRO.2020.120056.

58. Smadi, E.; Jafarian, M.; Dally, B.; Nathan, G.J. Steam Calcination of Lime for CO2 Capture. *J. Environ. Chem. Eng.* **2023**, *11*, 109812, doi:10.1016/J.JECE.2023.109812.
59. Muñoz, I.; Cifrian, E.; Andrés, A.; Miguel, G.S.; Ruiz, D.; Viguri, J.R. Analysis of Environmental Benefits Associated with the Incorporation of Waelz Slag into Fired Bricks Using LCA. *Constr. Build. Mater.* **2018**, *168*, 178–186, doi:10.1016/J.CONBUILDMAT.2018.02.108.
60. Georgiopoulou, M.; Lyberatos, G. Life Cycle Assessment of the Use of Alternative Fuels in Cement Kilns: A Case Study. *J. Environ. Manage.* **2018**, *216*, 224–234, doi:10.1016/J.JENVMAN.2017.07.017.
61. Yüksek, İ.; Öztaş, S.K.; Tahtalı, G. The Evaluation of Fired Clay Brick Production in Terms of Energy Efficiency: A Case Study in Turkey. *Energy Efficiency 2020 13:7* **2020**, *13*, 1473–1483, doi:10.1007/S12053-020-09896-Y.
62. Wolde, M.G.; Khatiwada, D.; Bekele, G.; Palm, B. A Life Cycle Assessment of Clinker and Cement Production in Ethiopia. *Cleaner Environmental Systems* **2024**, *13*, 100180, doi:10.1016/J.CESYS.2024.100180.
63. Zhang, X.; Biswas, W.K. Development of Eco-Efficient Bricks – A Life Cycle Assessment Approach. *Journal of Building Engineering* **2021**, *42*, 102429, doi:10.1016/J.JOBE.2021.102429.
64. Serpell, R.; Lopez, M. Reactivated Cementitious Materials from Hydrated Cement Paste Wastes. *Cem. Concr. Compos.* **2013**, *39*, 104–114, doi:10.1016/J.CEMCONCOMP.2013.03.020.
65. Ermilova, E.; Kamalova, Z. The Influence of Complex Additives Based on Calcined Clays and Carbonate Fillers on Hydration Products Composition of Blended Cement Stone. *E3S Web of Conferences* **2021**, *274*, 04004, doi:10.1051/e3sconf/202127404004.
66. Ye, G.; Liu, X.; De Schutter, G.; Poppe, A.M.; Taerwe, L. Influence of Limestone Powder Used as Filler in SCC on Hydration and Microstructure of Cement Pastes. *Cem. Concr. Compos.* **2007**, *29*, 94–102, doi:10.1016/j.cemconcomp.2006.09.003.
67. Scrivener, K.; Snellings, R.; Lothenbach, B. A Practical Guide to Microstructural Analysis of Cementitious Materials / Edited by Karen Scrivener, Ruben Snellings, Barbara Lothenbach. **2016**, 420–442.
68. Brandt, A.M.; Marks, M. Optimization of the Material Structure and Composition of Cement Based Composites. *Cem. Concr. Compos.* **1996**, *18*, 271–279, doi:10.1016/0958-9465(96)00018-2.
69. Poletto, M.; Zattera, A.J.; Santana, R.M.C. Thermal Decomposition of Wood: Kinetics and Degradation Mechanisms. *Bioresour. Technol.* **2012**, *126*, 7–12, doi:10.1016/J.BIORTECH.2012.08.133.

70. Boualleg, S.; Bencheikh, M.; Belagraa, L.; Daoudi, A.; Chikouche, M.A. The Combined Effect of the Initial Cure and the Type of Cement on the Natural Carbonation, the Portlandite Content, and Nonevaporable Water in Blended Cement. *Advances in Materials Science and Engineering* **2017**, *2017*, doi:10.1155/2017/5634713.
71. Fraga, L.G.; Silva, J.; Teixeira, S.; Soares, D.; Ferreira, M.; Teixeira, J. Influence of Operating Conditions on the Thermal Behavior and Kinetics of Pine Wood Particles Using Thermogravimetric Analysis. *Energies (Basel).* **2020**, *13*, 2756, doi:10.3390/en13112756.
72. Mohsen, A.; Aiad, I.; El-Hossiny, F.I.; Habib, A.O. Evaluating the Mechanical Properties of Admixed Blended Cement Pastes and Estimating Its Kinetics of Hydration by Different Techniques. *Egyptian Journal of Petroleum* **2020**, *29*, 171–186, doi:10.1016/j.ejpe.2020.03.001.
73. Santos, T.A.; De Oliveira Silva, G.A.E.; Ribeiro, D.V. Mineralogical Analysis of Portland Cement Pastes Rehydrated. *Journal of Solid Waste Technology and Management* **2020**, *46*, 15–23, doi:10.5276/JSWTM/2020.15.
74. Ifguis, O.; Moutcine, A.; Laghlimi, C.; Ziat, Y.; Bouhdadi, R.; Chtaini, A.; Moubarik, A.; Mbarki, M. Biopolymer-Modified Carbon Paste Electrode for the Electrochemical Detection of Pb(II) in Water. *J. Anal. Methods Chem.* **2022**, *2022*, doi:10.1155/2022/5348246.
75. Alonso, C.; Fernandez, L. Dehydration and Rehydration Processes of Cement Paste Exposed to High Temperature Environments. *J. Mater. Sci.* **2004**, *39*, 3015–3024, doi:10.1023/B:JMSC.0000025827.65956.18.
76. Kim, H.S.; Kim, S.; Kim, H.J.; Yang, H.S. Thermal Properties of Bio-Flour-Filled Polyolefin Composites with Different Compatibilizing Agent Type and Content. *Thermochim. Acta* **2006**, *451*, 181–188, doi:10.1016/J.TCA.2006.09.013.
77. Angelescu, N.; Stanciu, D.; Barroso de Aguiar, J.; Abdelgader, H.S.; Bratu, V. Role of Superplasticizer Additives Upon Hydration Process of Cement Pastes. *Scientific Bulletin of Valahia University - Materials and Mechanics* **2016**, *14*, 23–26, doi:10.1515/bsmm-2016-0004.
78. Santhanam, M.; Cohen, M.D.; Olek, J. Sulfate Attack Research - Whither Now? *Cem. Concr. Res.* **2001**, *31*, 845–851, doi:10.1016/S0008-8846(01)00510-5.
79. Kucharczyk, S.; Zajac, M.; Deja, J. The Influence of Limestone and Al2O3 Content in the Slag on the Performance of the Composite Cements. *Procedia Eng.* **2015**, *108*, 402–409, doi:10.1016/j.proeng.2015.06.164.
80. Habte, L.; Shiferaw, N.; Mulatu, D.; Thenepalli, T.; Chilakala, R.; Whan Ahn, J. Synthesis of Nano-Calcium Oxide from Waste Eggshell by Sol-Gel Method. *Sustainability* **2019**, *11*, 2–10.
81. Zhang, Q.; Ye, G. Dehydration Kinetics of Portland Cement Paste at High Temperature. *J. Therm. Anal. Calorim.* **2012**, *110*, 153–158, doi:10.1007/s10973-012-2303-9.

82. Zhang, Z.; Scherer, G.W. Evaluation of Drying Methods by Nitrogen Adsorption. *Cem. Concr. Res.* **2019**, *120*, 13–26, doi:10.1016/j.cemconres.2019.02.016.
83. Ermilova, E.; Kamalova, Z.; Ravil, R. Influence of Clay Mineral Composition on Properties of Blended Portland Cement with Complex Additives of Clays and Carbonates. *IOP Conf. Ser. Mater. Sci. Eng.* **2020**, *890*, doi:10.1088/1757-899X/890/1/012087.
84. Ghetti, P.; Ricca, L.; Angelini, L. Thermal Analysis of Biomass and Corresponding Pyrolysis Products. *Fuel* **1996**, *75*, 565–573, doi:10.1016/0016-2361(95)00296-0.
85. Devi, N.; Srivastava, S.; Yogi, B.; Gupta, S.K. A Review on Differential Thermal Analysis. *Chemistry Research Journal* **2021**, *f6*, 71–80.
86. Gabbott, Paul. *Principles and Applications of Thermal Analysis*; Blackwell Pub., 2008; ISBN 9781405131711.
87. Taylor, H.F.W. *Cement Chemistry*; Thomas Telford Publishing, 1997; ISBN 0-7277-3945-X.
88. Glasser, F.P.; Marchand, J.; Samson, E. Durability of Concrete — Degradation Phenomena Involving Detrimental Chemical Reactions. *Cem. Concr. Res.* **2008**, *38*, 226–246, doi:10.1016/J.CEMCONRES.2007.09.015.
89. Scrivener, K.L.; John, V.M.; Gartner, E.M. Eco-Efficient Cements: Potential Economically Viable Solutions for a Low-CO2 Cement-Based Materials Industry. *Cem. Concr. Res.* **2018**, *114*, 2–26, doi:10.1016/J.CEMCONRES.2018.03.015.
90. Le Saoût, G.; Lothenbach, B.; Hori, A.; Higuchi, T.; Winnefeld, F. Hydration of Portland Cement with Additions of Calcium Sulfoaluminates. *Cem. Concr. Res.* **2013**, *43*, 81–94, doi:10.1016/J.CEMCONRES.2012.10.011.
91. Villain, G.; Thiery, M.; Platret, G. Measurement Methods of Carbonation Profiles in Concrete: Thermogravimetry, Chemical Analysis and Gammadensimetry. *Cem. Concr. Res.* **2007**, *37*, 1182–1192, doi:10.1016/J.CEMCONRES.2007.04.015.
92. Pane, I.; Hansen, W. Investigation of Blended Cement Hydration by Isothermal Calorimetry and Thermal Analysis. *Cem. Concr. Res.* **2005**, *35*, 1155–1164, doi:10.1016/J.CEMCONRES.2004.10.027.
93. Mumme, W.; Hill, R.J.; Bushnell-wye, G.; Segnit, E. Rietveld Crystal Structure Refinements, Crystal Chemistry and Calculated Powder Diffraction Data for the Polymorphs of Dicalcium Silicate and Related Phases. **1995**.
94. Chatterjee, A.K. High Belite Cements—Present Status and Future Technological Options: Part I. *Cem. Concr. Res.* **1996**, *26*, 1213–1225, doi:10.1016/0008-8846(96)00099-3.
95. Aranda, M.A.G.; De la Torre, A.G. Sulfoaluminate Cement. *Eco-Efficient Concrete* **2013**, 488–522, doi:10.1533/9780857098993.4.488.

96. Hanein, T.; Galvez-Martos, J.L.; Bannerman, M.N. Carbon Footprint of Calcium Sulfoaluminate Clinker Production. *J. Clean. Prod.* **2018**, *172*, 2278–2287, doi:10.1016/J.JCLEPRO.2017.11.183.
97. Shui, Z.; Xuan, D.; Wan, H.; Cao, B. Rehydration Reactivity of Recycled Mortar from Concrete Waste Experienced to Thermal Treatment. *Constr. Build. Mater.* **2008**, *22*, 1723–1729, doi:10.1016/J.CONBUILDMAT.2007.05.012.
98. Alarcon-Ruiz, L.; Platret, G.; Massieu, E.; Ehrlacher, A. The Use of Thermal Analysis in Assessing the Effect of Temperature on a Cement Paste. *Cem. Concr. Res.* **2005**, *35*, 609–613, doi:10.1016/J.CEMCONRES.2004.06.015.
99. Matschei, T.; Lothenbach, B.; Glasser, F.P. Thermodynamic Properties of Portland Cement Hydrates in the System CaO-Al2O3-SiO2-CaSO4-CaCO3-H2O. *Cem. Concr. Res.* **2007**, *37*, 1379–1410, doi:10.1016/J.CEMCONRES.2007.06.002.
100. Zajac, M.; Skocek, J.; Bullerjahn, F.; Ben Haha, M. Effect of Retarders on the Early Hydration of Calcium-Sulpho-Aluminate (CSA) Type Cements. *Cem. Concr. Res.* **2016**, *84*, 62–75, doi:10.1016/J.CEMCONRES.2016.02.014.
101. Ben Haha, M.; Winnefeld, F.; Pisch, A. Advances in Understanding Ye'elimite-Rich Cements. *Cem. Concr. Res.* **2019**, *123*, 105778, doi:10.1016/J.CEMCONRES.2019.105778.
102. Kaufmann, J.; Winnefeld, F.; Hesselbarth, D. Effect of the Addition of Ultrafine Cement and Short Fiber Reinforcement on Shrinkage, Rheological and Mechanical Properties of Portland Cement Pastes. *Cem. Concr. Compos.* **2004**, *26*, 541–549, doi:10.1016/S0958-9465(03)00070-2.
103. Tural, H.G.; Ozarisoy, B.; Derogar, S.; Ince, C. Investigating the Governing Factors Influencing the Pozzolanic Activity through a Database Approach for the Development of Sustainable Cementitious Materials. *Constr. Build. Mater.* **2024**, *411*, 134253, doi:10.1016/J.CONBUILDMAT.2023.134253.
104. Abd elaty, M. abd allah Compressive Strength Prediction of Portland Cement Concrete with Age Using a New Model. *HBRC Journal* **2014**, *10*, 145–155, doi:10.1016/j.hbrcj.2013.09.005.
105. Gholizadeh-Vayghan, A.; Meza Hernandez, G.; Kingne, F.K.; Gu, J.; Dilissen, N.; El Kadi, M.; Tysmans, T.; Vleugels, J.; Rahier, H.; Snellings, R. Thermal Reactivation of Hydrated Cement Paste: Properties and Impact on Cement Hydration. *Materials 2024, Vol. 17,* **2024**, *17*, doi:10.3390/ma17112659.
106. Zanovello Sérgio Angulo, M.; composto, C.T.; Zanovello, M. Thermoactivated Recycled Cement Waste: Optimal Dehydration Temperature and Binder Properties Insights. *Ambiente Construído* **2025**, *25*, e143282, doi:10.1590/s1678-86212025000100889.
107. Mordor Intelligence *Cement Board Market - Share & Size*; 2024;